

1

1 **Massively integrated coexpression**  
2 **analysis reveals transcriptional**  
3 **regulation, evolution and cellular**  
4 **implications of the noncanonical**  
5 **translatome**

6 **April Rich<sup>+1,2,3</sup>, Omer Acar<sup>+1,2,3</sup>, Anne-Ruxandra Carvunis<sup>\*2,3</sup>**

7 <sup>1</sup>*Joint Carnegie Mellon University-University of Pittsburgh Computational Biology PhD Program,*

8 *University of Pittsburgh, Pittsburgh, PA, USA;* <sup>2</sup>*Department of Computational and Systems*

9 *Biology, University of Pittsburgh School of Medicine, Pittsburgh, PA, USA;* <sup>3</sup>*Pittsburgh Center for*

10 *Evolutionary Biology and Medicine (CEBaM), University of Pittsburgh, Pittsburgh, PA, USA*

11 <sup>+</sup> co-first authors

12 <sup>\*</sup> corresponding author

14

3

## 15 Abstract

### 16 **Background:**

17 Recent studies uncovered pervasive transcription and translation of thousands of noncanonical  
18 open reading frames (nORFs) outside of annotated genes. The contribution of nORFs to cellular  
19 phenotypes is difficult to infer using conventional approaches because nORFs tend to be short,  
20 of recent *de novo* origins, and lowly expressed. Here we develop a dedicated coexpression  
21 analysis framework that accounts for low expression to investigate the transcriptional regulation,  
22 evolution, and potential cellular roles of nORFs in *Saccharomyces cerevisiae*.

### 23 **Results:**

24 Our results reveal that nORFs tend to be preferentially coexpressed with genes involved in  
25 cellular transport or homeostasis but rarely with genes involved in RNA processing.  
26 Mechanistically, we discover that young *de novo* nORFs located downstream of conserved  
27 genes tend to leverage their neighbors' promoters through transcription readthrough, resulting in  
28 high coexpression and high expression levels. Transcriptional piggybacking also influences the  
29 coexpression profiles of young *de novo* nORFs located upstream of genes, but to a lesser  
30 extent and without detectable impact on expression levels. Transcriptional piggybacking  
31 influences, but does not determine, the transcription profiles of *de novo* nORFs emerging  
32 nearby genes. About 40% of nORFs are not strongly coexpressed with any gene but are  
33 transcriptionally regulated nonetheless and tend to form entirely new transcription modules. We  
34 offer a web browser interface (<https://carvunislab.csb.pitt.edu/shiny/coexpression/>) to efficiently  
35 query, visualize and download our coexpression inferences.

### 36 **Conclusions:**

5

37 Our results suggest that nORF transcription is highly regulated. Our coexpression dataset  
38 serves as an unprecedented resource for unraveling how nORFs integrate into cellular  
39 networks, contribute to cellular phenotypes, and evolve.

40 **Keywords:**

41 Coexpression networks, de novo gene birth, noncanonical ORFs, translatome, smORFs,  
42 transcriptional regulation

## 43 Background

44 Eukaryotic genomes encompass thousands of open reading frames (ORFs). The vast majority  
45 are so-called “noncanonical” ORFs (nORFs) excluded from genome annotations because of  
46 their short length, lack of evolutionary conservation, and perceived irrelevance to cellular  
47 physiology [1–3]. The development of RNA sequencing (RNA-seq) [4] and ribosome profiling  
48 [5,6] has revealed genome-wide transcription and translation of nORFs across species ranging  
49 from yeast to humans [6–14]. Recent studies have characterized individual nORFs that form  
50 stable peptides and impact phenotypes, including cell growth [10,13,15], cell cycle regulation  
51 [16], muscle physiology [17–19], and immunity [20–22]. Unraveling the cellular, physiological  
52 and evolutionary implications of nORFs has become an active area of research [14,23].

53

54 Many nORFs have evolved *de novo* from previously noncoding regions [24–26]. Thus, the study  
55 of nORFs and *de novo* gene birth as evolutionary innovation carries a synergistic overlap where  
56 findings in one area could improve our understanding of the other. For instance, Sandmann et  
57 al. measured physical protein interactions for hundreds of peptides translated from nORFs and  
58 proposed that short linear motifs present in young *de novo* nORFs could mediate how nORFs  
59 impact essential cellular processes [26]. Other studies observed a gradual integration of

7

60 evolutionary young ORFs into cellular networks and showed they could gain essential roles [27–  
61 29]. These studies support an evolutionary model whereby pervasive expression of nORFs  
62 generates the raw material for *de novo* gene birth [24,25].

63

64 The biological interpretation of nORF expression is complex. Some studies suggest that the  
65 transcription or translation of nORFs could be attributed to expression noise [30–32], whereby  
66 non-specific binding of RNA polymerases and ribosomes to DNA and RNA might cause  
67 promiscuous transcription or translation, respectively. How do nORFs become expressed in the  
68 first place? There are multiple hypotheses on how *de novo* ORFs gain the ability to become  
69 transcriptionally regulated [33]. One possibility is the emergence of novel regulatory regions  
70 along with or following the emergence of an ORF (ORF-first), as was shown for specific *de novo*  
71 ORFs in *Drosophila melanogaster* [34], codfish [35], human [36,37] and chimpanzee [36].  
72 Alternatively, ORFs may emerge on actively transcribed loci such as near enhancers [38] or on  
73 long noncoding RNAs [39], as was shown for *de novo* ORFs in primates [40] and for *de novo*  
74 ORFs upstream or downstream of transcripts containing genes [37] (transcription-first) [41–43].  
75 Transcription has a ripple effect causing coordinated activation of nearby genes [44,45]. Thus,  
76 *de novo* ORFs that emerge near established genes or regulatory regions may acquire  
77 transcriptional regulation by ‘piggybacking’ [45] on the pre-existing regulatory context [41,46].  
78 This piggybacking could predispose *de novo* ORFs to be involved in similar cellular processes  
79 as their neighbors, which in turn would help with characterization. To date, the fraction of  
80 nORFs that are transcriptionally regulated and contribute to cellular phenotypes is unknown for  
81 any species.

82

83 An obstacle to studying nORF expression at scale is their detection, as nORF expression levels  
84 are typically low and reliant on specific conditions [24,36]. Recent studies demonstrated that the

9

85 integration of omics data [14,47–49] could effectively address detection issues. For example,  
86 Wacholder et al. [14] recently discovered around 19,000 translated nORFs in *Saccharomyces*  
87 *cerevisiae* by massive integration of ribosome profiling data. This figure is three times larger  
88 than the number of canonical ORFs (cORFs) annotated in the yeast genome. These translated  
89 nORFs have the potential to generate peptides that affect cellular phenotypes but are almost  
90 entirely uncharacterized.

91

92 Coexpression is a well-established approach for studying transcriptional regulation through the  
93 massive integration of RNA-seq data. Coexpression refers to the similarity between  
94 transcriptional profiles of ORF pairs across numerous samples. Coexpression has been used  
95 successfully to identify new gene functions [50,51], disease-related genes [22,52,53] and for  
96 studying the conservation of the regulatory machinery [51,54] or gene modules [55] between  
97 species. Based on the assumption that genes involved in similar pathways have correlated  
98 expression patterns, coexpression can reveal relationships between genes and other  
99 transcribed genetic elements [56,57]. Most coexpression studies have focused on cORFs, but  
100 the abundance of publicly available RNA-seq data represents a tractable avenue to interrogate  
101 the transcriptional regulation of thousands of nORFs at once using coexpression approaches  
102 [47,58–61]. Indeed, RNA-seq is probe-agnostic and annotation-agnostic, thereby enabling the  
103 reuse of existing data to explore these novel ORFs. However, low expression levels can distort  
104 coexpression inferences due to statistical biases [62,63]. A coexpression analysis of translated  
105 nORFs that addresses the statistical issues arising from low expression is still lacking for any  
106 species.

107

108 Here, we developed a dedicated statistical approach that accounts for low expression levels  
109 when inferring coexpression relationships between ORFs. We applied this approach to the  
110 recently identified 19,000 translated nORFs in *S. cerevisiae* [14] and built the first high-quality

11

111 coexpression network spanning the canonical and noncanonical translatome of any species.  
112 Coexpression relationships suggest that the majority of nORFs are transcriptionally regulated.  
113 While many nORFs form entirely new noncanonical transcription modules, approximately half  
114 are transcriptionally associated with genes involved in cellular homeostasis and transport. We  
115 show that *de novo* ORFs that piggyback onto their neighbors' transcription tend to have higher  
116 expression and tend to be highly coexpressed with their neighbors. We provide a web  
117 application to allow researchers to easily access this dataset to investigate the coexpression  
118 relationships and potential cellular roles for thousands of ORFs.

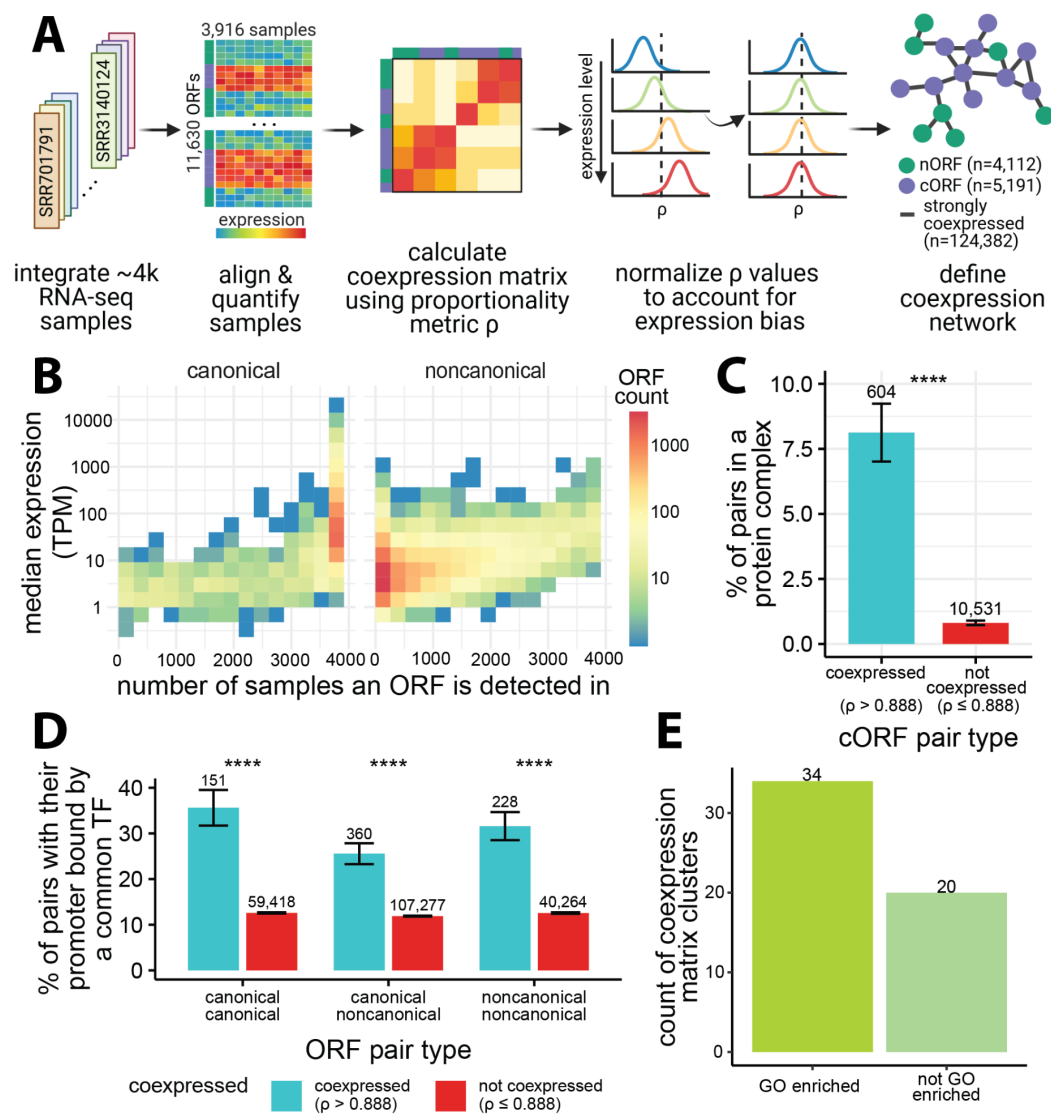
12

6

13

## 119 Results

### 120 High-quality coexpression inferences show transcriptional and 121 regulatory relationships between nORFs and cORFs



122

123 **Figure 1: Overview of coexpression inference framework and properties of the dataset**

15

124 A) Workflow: 3,916 samples were analyzed to create an expression matrix for 11,630 ORFs,  
125 including 5,803 cORFs and 5,827 nORFs; center log ratio transformed (clr) expression values  
126 were used to calculate the coexpression matrix using proportionality metric,  $\rho$ , followed by  
127 normalization to correct for expression bias. The coexpression matrix was thresholded using  $\rho >$   
128 0.888 to create a coexpression network (top 0.2% of all pairs). B) Distribution of the number of  
129 ORFs binned based on their median expression values (transcript per million - TPM) and the  
130 number of samples the ORFs were detected in with at least 5 raw counts. C) Coexpressed  
131 cORF pairs ( $\rho > 0.888$ ) are more likely to encode proteins that form complexes than non-  
132 coexpressed cORF pairs (Fisher's exact test  $p < 2.2e-16$ ; error bars: standard error of the  
133 proportion); using annotated protein complexes from ref. [64]. D) Coexpressed ORF pairs ( $\rho >$   
134 0.888) are more likely to have their promoters bound by a common transcription factor (TF) than  
135 non-coexpressed ORF pairs (Fisher's exact test  $p < 2.2e-16$ ; error bars: standard error of the  
136 proportion); genome-wide TF binding profiles from ref. [65] and transcription start sites (TSS)  
137 from ref. [66] were analyzed to define promoter binding (see Methods). E) Hierarchical  
138 clustering of the coexpression matrix reveals functional enrichments for most clusters that  
139 contain at least 5 cORFs; functional enrichments estimated by gene ontology (GO) enrichment  
140 analysis at false discovery rate (FDR)  $< 0.05$  using Fisher's exact test.

141

142 To infer coexpression at the translatome scale in *S. cerevisiae*, we considered all cORFs  
143 annotated as "verified", "uncharacterized", or "transposable element" in the *Saccharomyces*  
144 Genome Database (SGD) [67], as well as all nORFs, ORFs that were either unannotated or  
145 annotated as "dubious" and "pseudogene", with evidence of translation according to Wacholder  
146 et al. [14]. To maximize detection of transcripts containing nORFs, we curated and integrated  
147 3,916 publicly available RNA-seq samples from 174 studies (Figure 1A, Supplementary Data 1).  
148 Many nORFs were not detected in most of the samples we collected, creating a very sparse  
149 dataset (Figure 1B). The issue of sparsity has been widely studied in the context of single cell

17

150 RNA-seq (scRNA-seq). A recent study looking at multiple measures of association for  
151 constructing coexpression networks from scRNA-seq showed that proportionality methods  
152 coupled with center log ratio (clr) transformation consistently outperformed other measures of  
153 coexpression in a variety of tasks including identification of disease-related genes and protein-  
154 protein network overlap analysis [68]. Thus, we used clr to transform the raw read counts and  
155 quantified coexpression relationships using the proportionality metric,  $\rho$  [69].

156

157 We further addressed the issue of sparsity with two sample thresholding approaches. First, any  
158 observation with a raw count below five was discarded, such that when calculating  $\rho$  only the  
159 samples expressing both ORFs with at least five counts were considered. Second, we  
160 empirically determined that a minimum of 400 samples were required to obtain reliable  
161 coexpression values by assessing the effect of sample counts on the stability of  $\rho$  values  
162 (Supplementary Figure 1). These steps resulted in an 11,630 by 11,630 coexpression matrix  
163 encompassing 5,803 cORFs and 5,827 nORFs (ORF list in Supplementary Data 2).

164

165 The combined use of clr,  $\rho$ , and sample thresholding accounted for statistical issues in  
166 estimating coexpression deriving from sparsity, but the large difference in RNA expression  
167 levels between cORFs and nORFs posed yet another challenge. Indeed, Wang et al. showed  
168 that the distribution of coexpression values is biased by expression level due to statistical  
169 artifacts [62]. We observed this artifactual bias in our dataset (Supplementary Figure 2A) and  
170 corrected for it using spatial quantile normalization (SpQN) as recommended by Wang et al. [62]  
171 (Supplementary Figure 2B). This resulted in a normalized coexpression matrix (Supplementary  
172 Data 3) with  $\rho$  values centered around 0.476.

173

174 We then created a network representation of the coexpression matrix by considering only the  
175 top 0.2% of  $\rho$  values between all ORF pairs ( $\rho > 0.888$ ). This threshold was chosen to include

19

176 90% of cORFs (Supplementary Figure 3). Altogether, our dedicated analysis framework (Figure  
177 1A) inferred 124,382 strong ( $p > 0.888$ ) coexpression relationships between 9,303 ORFs,  
178 encompassing 4,112 nORFs and 5,191 cORFs.

179

180 To assess whether our coexpression network captures meaningful biological and regulatory  
181 relationships, we examined its overlap with orthogonal datasets. Using a curated [64] protein  
182 complex dataset for cORFs, we found that coexpressed cORF pairs are significantly more likely  
183 to encode proteins that form a protein complex together compared to non-coexpressed pairs  
184 (Odds ratio = 10.8 Fisher's exact test  $p < 2.2e-16$ ; Figure 1C). Using a previously published [65]  
185 genome-wide chromatin immunoprecipitation with exonuclease digestion (ChIP-exo) dataset  
186 containing DNA-binding information for 73 sequence-specific transcription factors (TFs) and  
187 using transcript isoform sequencing (TIF-seq) [66] data to determine transcription start sites  
188 (TSSs) and promoter regions, we observed that coexpressed ORF pairs were more likely to  
189 have their promoters bound by a common TF than non-coexpressed ORF pairs, whether the  
190 pairs consist of nORFs or cORFs (*canonical-canonical pairs*: Odds ratio = 3.84, *canonical-*  
191 *noncanonical pairs*: Odds ratio = 2.55, *noncanonical-noncanonical pairs*: Odds ratio = 3.22,  
192 Fisher's exact test  $p < 2.2e-16$  for all three comparisons; Figure 1D). Enrichments were robust  
193 to different coexpression cutoffs (Supplementary Figure 4-5). Using the WGCNA [70] method to  
194 cluster the coexpression matrix, we found that more than half of the clusters identified contained  
195 functionally related ORFs (gene ontology (GO) biological process enrichments at Benjamini-  
196 Hochberg (BH) adjusted false discovery rate (FDR)  $< 0.05$ ; Figure 1E; Supplementary Figure 6).  
197 These analyses demonstrate the high quality of our coexpression network and confirm that it  
198 captures meaningful biological and regulatory relationships for both cORFs and nORFs.

199

200 Conventional approaches for coexpression analysis include using transcript per million (TPM) or  
201 reads per kilobase per million (RPKM) normalization, batch correction by removing top principal

20

10

21

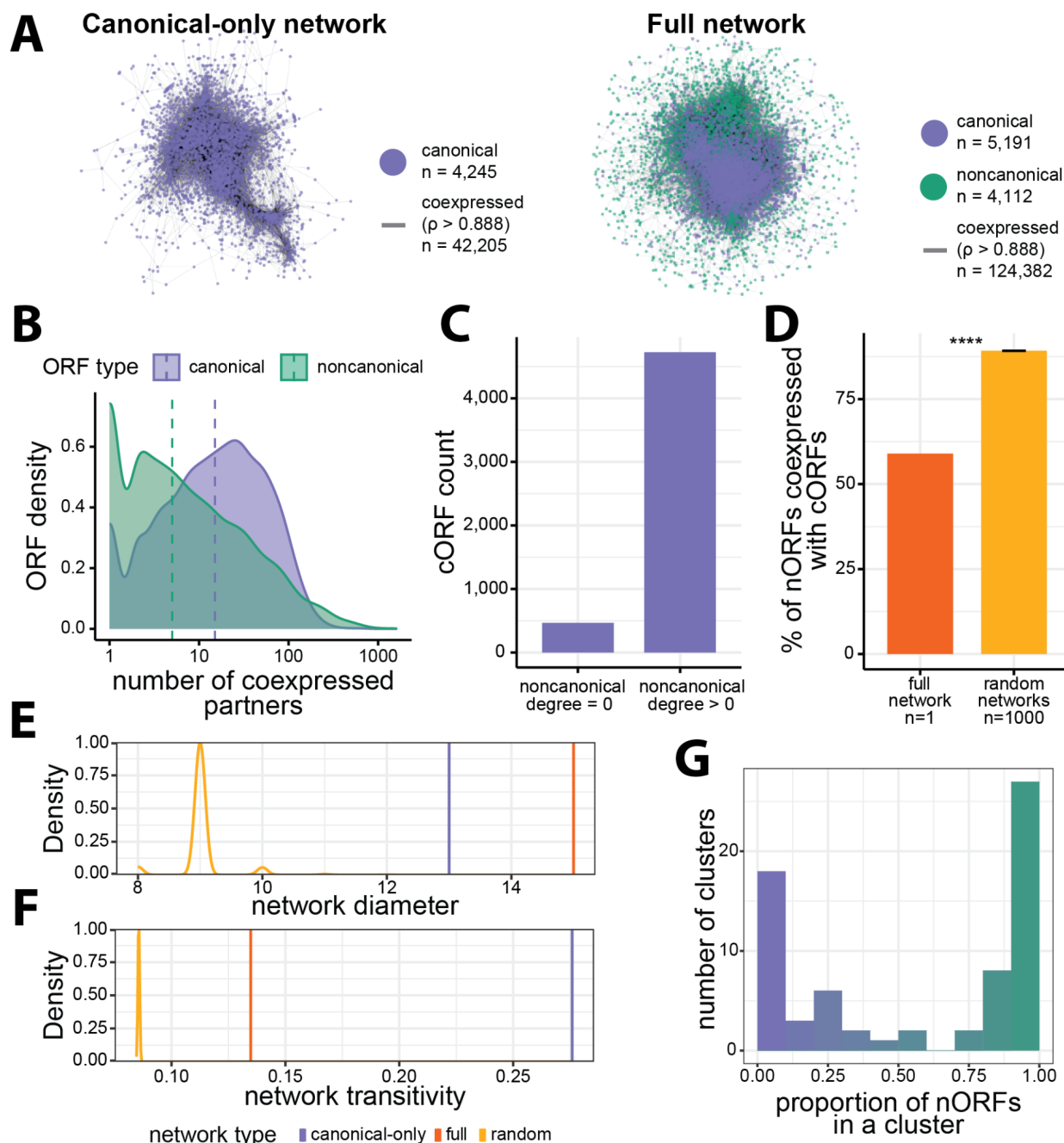
202 components, and Pearson's correlation as the similarity metric [71,56,72]. Compared to these  
203 approaches, our framework increased the proportion of coexpressed ORF pairs whose  
204 promoters are bound by a common TF specifically for pairs containing nORFs (Supplementary  
205 Figure 7), and yielded coexpression networks encompassing the largest number of nORFs at  
206 most thresholds (Supplementary Figure 8). Hence our dedicated analysis framework therefore  
207 outperforms conventional coexpression approaches for the study of nORFs. We offer an R  
208 Shiny [73] interface (<https://carvunislab.csb.pitt.edu/shiny/coexpression/>) to efficiently query,  
209 visualize and download the coexpression data we generated. To our knowledge, this is the most  
210 comprehensive coexpression dataset focusing on empirically translated elements, both  
211 annotated and unannotated, for any species to date.

22

11

23

212 nORFs tend to be located at the periphery of the coexpression  
213 network and form new noncanonical transcription modules



214

215 **Figure 2 Topological properties of the coexpression network**

24

12

25

216 A) Visualization for canonical-only and full coexpression networks using spring embedded graph  
217 layout [74]. The full network contains more cORFs than the canonical-only network since  
218 addition of nORFs also results in addition of many cORFs that are only connected to an nORF.  
219 B) nORFs have fewer coexpression partners (degree in full network) than cORFs (Mann-  
220 Whitney U-test  $p < 2.2e-16$ ). C) Most cORFs are coexpressed with at least one nORF. D) Only  
221 59% of nORFs are coexpressed with at least one cORFs and this is less than expected by  
222 chance, on average, 89% of nORFs are coexpressed with a cORF across 1,000 randomized  
223 networks generated in a degree-preserving fashion by swapping edges of noncanonical nodes  
224 (Fisher's exact test  $p < 2.2e-16$ ; error bar: standard error of the mean proportion across  
225 randomized networks). E) Addition of nORFs to the canonical-only network results in the full  
226 network being less compact, whereas the opposite is expected by chance, shown by the  
227 decrease in diameters for the 1,000 randomized networks. F) Addition of nORFs to the  
228 canonical-only network decreases local clustering in the full network, however this is to a lesser  
229 extent than expected by chance as shown by the distribution for the 1,000 randomized  
230 networks. G) Most clusters in the coexpression matrix encompass either primarily nORFs or  
231 primarily cORFs (n= 69 clusters, *green* represents nORF majority clusters, *purple* represents  
232 cORF majority clusters).

233

234 Conventional analyses of coexpression networks have been restricted to cORFs. Our full  
235 coexpression network contains twice the number of ORFs and three times the number of strong  
236 ( $\rho > 0.888$ ) coexpression relationships compared to the canonical-only network (Figure 2A). We  
237 sought to compare the network properties of the canonical-only and full networks. On average,  
238 nORFs have fewer coexpressed partners (degree) than cORFs, suggesting that nORFs have  
239 distinct transcriptional profiles (Cliff's Delta  $d = -0.29$ , Mann-Whitney U-test  $p < 2.2e-16$ ; Figure  
240 2B). We found that 91% of cORFs are coexpressed with at least one nORF ( $n = 4,726$ ; Figure  
241 2C), whereas only 59% of nORFs are coexpressed with at least one cORF. In contrast, we

26

13

27

242 would have expected an average of 89% of nORFs to be coexpressed with a cORF according  
243 to degree preserving simulations of 1,000 randomized networks where edges from nORFs were  
244 shuffled (Odds ratio = 0.174, Fisher's exact test  $p < 2.2\text{e-}16$ ; Figure 2D, Supplementary Figure  
245 9). This suggests that, while most nORFs are integrated in the full coexpression network, they  
246 also have distinct expression profiles that differ markedly from those of all cORFs and are more  
247 similar to those of other nORFs.

248

249 To investigate how these seemingly conflicting attributes impact the organization of the  
250 coexpression network, we analyzed two global network properties: diameter, which is the  
251 longest shortest path between any two ORFs; and transitivity, which is the tendency for ORFs  
252 that are coexpressed with a common neighbor to also be coexpressed with each other. The  
253 incorporation of nORFs in the full network led to a larger diameter relative to the canonical-only  
254 network (Figure 2E). This is in sharp contrast with the null expectation, set by 1,000 degree-  
255 preserving simulations, whereby random incorporation of nORFs decreases network diameter.  
256 The full coexpression network is thus much less compact than expected by chance, suggesting  
257 that nORFs tend to be located at the periphery of the network. Network transitivity decreased  
258 with the incorporation of nORFs compared to the canonical-only network, but to a lesser extent  
259 than expected by chance (Figure 2F). This suggests that despite their low degree and  
260 peripheral locations, the connections formed by nORFs are structured and may form  
261 noncanonical clusters.

262

263 To investigate this hypothesis, we inspected the ratio of nORFs and cORFs among the cluster  
264 assignments from WGCNA hierarchical clustering of the full coexpression matrix  
265 (Supplementary Figure 6). Strikingly, we observed a bimodal distribution of clusters, with  
266 approximately half of the clusters consisting mostly of nORFs and the other half containing  
267 mostly cORFs (Figure 2G). We conclude that nORFs exhibit a unique and non-random

29

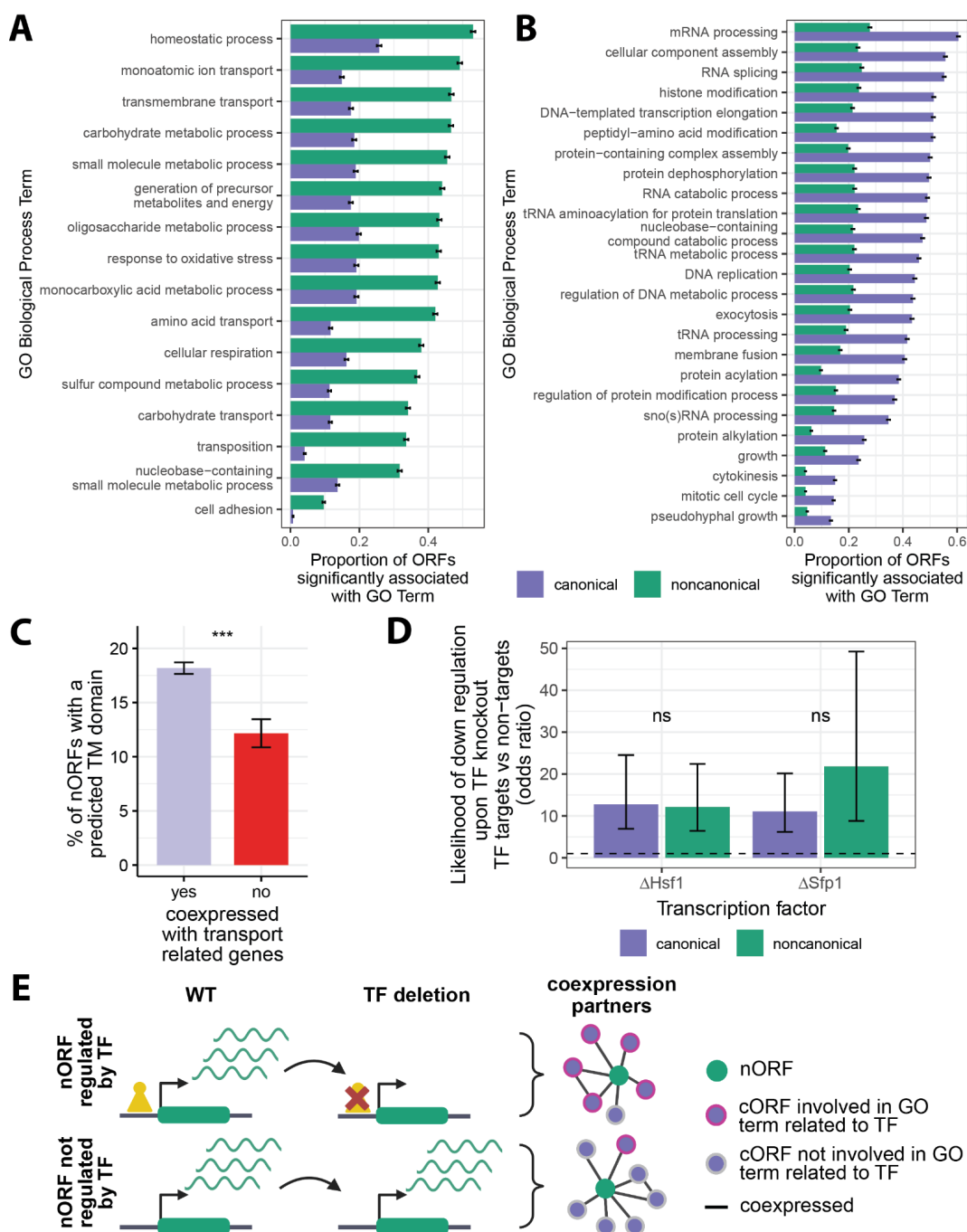
268 organization within the coexpression network, simultaneously connecting to all cORFs while  
269 also forming entirely new noncanonical transcription modules.

30

15

31

270 Coexpression profiles reveal most nORFs are transcriptionally  
 271 associated with genes involved in cellular transport and  
 272 homeostasis



273

33

274 **Figure 3 Biological processes associated with nORF transcriptional regulation**

275 A-B) Biological processes that are more (A) (Odds ratio > 2, n = 16 terms) or less (B) (Odds  
276 ratio < 0.5, n = 23 terms) transcriptionally associated with nORFs than cORFs (y-axis ordered  
277 by nORF enrichment proportion from highest to lowest, BH adjusted FDR < 0.001 for all terms,  
278 Fisher's exact test, GO term enrichments were detected using gene set enrichment analyses  
279 (GSEA), error bars: standard error of the proportion). C) nORFs that are highly coexpressed  
280 with genes involved in transport are more likely to have predicted transmembrane (TM) domains  
281 as determined by TMHMM [75] compared to nORFs that are not (Odds ratio = 1.6, Fisher's  
282 exact test p = 1.3e-4; error bars: standard error of the proportion). D) nORFs and cORFs that  
283 are Sfp1 or Hsf1 targets are more likely to be downregulated when Sfp1 or Hsf1 are deleted  
284 compared to ORFs that are not targets (Sfp1: cORFs: p < 2.2e-16; nORFs: p = 2.8e-9; Hsf1:  
285 cORFs: p < 2.2e-16; nORFs: p = 9.9e-13; Fisher's exact test, error bars: 95% confidence interval  
286 of the odds ratio; *dashed* line shows odds ratio of 1; RNA abundance data from SRA accession  
287 SRP159150 and SRP437124 [76] respectively). E) nORFs that are regulated by TFs are more  
288 likely to be coexpressed with genes involved in processes related to known functions of that TF.  
289

290 To determine whether nORFs are transcriptionally associated with specific cellular processes,  
291 we performed gene set enrichment analyses [77] (GSEA) on their coexpression partners. GSEA  
292 takes an ordered list of genes, in this case sorted by coexpression level, and seeks to find if the  
293 higher ranked genes are preferentially annotated with specific GO terms. For each cORF and  
294 nORF, we ran GSEA to detect if their highly coexpressed partners were preferentially  
295 associated with any GO terms (Supplementary Figure 10). Almost all ORFs (99.9%), whether  
296 cORF or nORF, had at least one significant GO term associated with their coexpression  
297 partners at BH adjusted FDR < 0.01, suggesting that nORFs are engaged in coherent  
298 transcriptional programs. We then calculated, for each GO term, the number of cORFs and

35

299 nORFs with GSEA enrichments in this term (Supplementary Data 4). These analyses identified  
300 specific GO terms that were significantly more (16 terms, BH adjusted FDR < 0.001, Odds ratio  
301 > 2, Fisher's exact test; Figure 3A, Supplementary Data 5) or less (23 terms, BH adjusted FDR  
302 < 0.001, Odds ratio < 2, Fisher's exact test; Figure 3B, Supplementary Data 5) prevalent among  
303 the coexpression partners of nORFs relative to those of cORFs. Most of the GO terms that were  
304 significantly enriched among the coexpression partners of nORFs were related to cellular  
305 homeostasis and transport (Figure 3A) while most of the GO terms significantly depleted among  
306 the coexpression partners of nORFs were related to DNA, RNA, and protein processing (Figure  
307 3B). Running the same GSEA pipeline with Kyoto Encyclopedia of Genes and Genomes  
308 (KEGG) [78] annotations yielded consistent results (Supplementary Figure 11, Supplementary  
309 Data 6-7). Half of nORFs were coexpressed with genes involved in homeostasis (GO:0042592,  
310 53%), monoatomic ion transport (GO:0006811, 49%) and transmembrane transport  
311 (GO:0055085, 47%). The nORFs transcriptionally associated with the parent term 'transport' (n  
312 = 2,718, GO:0006810, GSEA BH adjusted FDR < 0.01) were 1.6 times more likely to contain a  
313 predicted transmembrane domain than other nORFs (p = 1.3e-4, Fisher's exact test; Figure 3C),  
314 in line with potential transport-related activities. These findings reveal a strong and previously  
315 unsuspected transcriptional association between nORFs, and cellular processes related to  
316 homeostasis and transport.

317 **Hsf1 and Sfp1 nORF targets are part of protein folding and  
318 ribosome biogenesis transcriptional programs, respectively**

319 Overall, our analyses relating coexpression to TF binding (Figure 1D) and functional  
320 enrichments (Figure 3A-B) suggest that nORF expression is regulated rather than simply the  
321 consequence of transcriptional noise. To further investigate this hypothesis, we sought to  
322 identify regulatory relationships between specific TFs and nORFs. We reasoned that if nORFs

37

323 are regulated by TFs in similar ways as cORFs, then genetic knockout of the TFs that regulate  
324 them should impact their expression levels as it does for cORFs [79]. We focused on two  
325 transcriptional activators for which both ChIP-exo [65] and knockout RNA-seq data [76] were  
326 publicly available: Sfp1, which regulates ribosome biogenesis [80] and Hsf1, which regulates  
327 heat shock and protein folding responses [81].

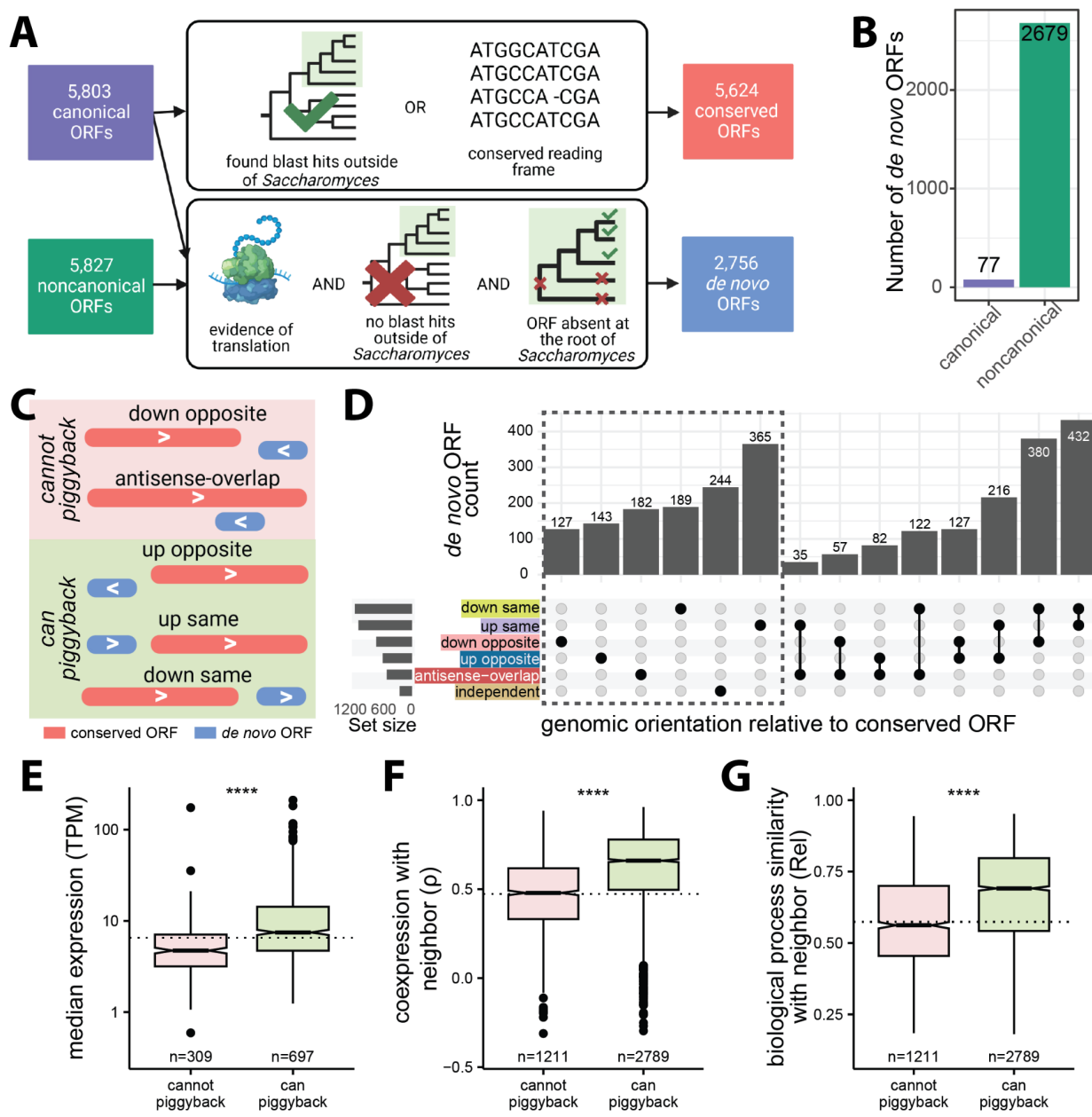
328

329 For both cORFs and nORFs, knockout of Sfp1 or Hsf1 was more likely to trigger a significant  
330 decrease in expression when the ORF's promoter was bound by the respective TF according to  
331 ChIP-exo evidence (Figure 3D). The statistical association between TF binding and knockout-  
332 induced downregulation was as strong for nORFs as it was for cORFs, consistent with nORFs  
333 having similar mechanisms of transcriptional activation (*Sfp1*: cORFs Odds ratio = 11.1,  $p <$   
334 2.2e-16; nORFs Odds ratio = 21.8,  $p = 2.8e-9$ , Fisher's exact test; *Hsf1*: cORFs Odds ratio =  
335 12.7,  $p < 2.2e-16$ ; nORFs Odds ratio = 12.1,  $p = 9.9e-13$ , Fisher's exact test). Therefore, the  
336 nORFs whose promoters are bound by these TFs, and whose expression levels decrease upon  
337 deletion of these TFs, are likely genuine regulatory targets of these TFs. By this stringent  
338 definition, our analyses identified 9 nORF targets of Sfp1 (and 34 cORF targets) and 19 nORF  
339 targets of Hsf1 (and 39 cORF targets). The coexpression profiles of these Sfp1 and Hsf1 nORF  
340 targets were preferentially associated with genes involved in processes directly related to the  
341 known functions of Sfp1 and Hsf1 (Supplementary Data 8). For example, the coexpression  
342 profiles of 9 Sfp1 nORF targets revealed preferential associations with genes involved in  
343 'ribosomal large subunit biogenesis' and 7 Sfp1 nORF targets involved in 'regulation of  
344 translation' according to our GSEA pipeline (Fisher's exact test, BH adjusted  $p$ -value  $< 6.7e-4$   
345 for both terms). Similarly, 13 Hsf1 nORF targets were preferentially associated with genes  
346 involved in 'Protein Folding' (Fisher's exact test, BH adjusted  $p$ -value = 5.7e-9). These results

39

347 show that nORF expression can be actively regulated by TFs as part of coherent transcriptional  
 348 programs (Figure 3E).

349 *de novo* ORF expression and regulation are shaped by genomic  
 350 location



351

41

352 **Figure 4 Expression, coexpression and biological processes similarity of *de novo* ORFs**  
353 **with respect to genomic orientations**

354 A) Pipeline used to reclassify ORFs as conserved or *de novo*. cORFs were considered for both  
355 conserved and *de novo* classification while nORFs were only considered for *de novo*  
356 classification. Conserved ORFs were determined by either detection of homology outside of  
357 *Saccharomyces* or reading frame conservation within *Saccharomyces* (*top*). *De novo* ORFs  
358 were determined by evidence of translation, lack of homology outside of *Saccharomyces* as well  
359 as lack of a homologous ORF in the two most distant *Saccharomyces* branches (*bottom*). B)  
360 Counts of cORFs and nORFs that emerged *de novo*. C) Genomic orientations of *de novo* ORFs  
361 that cannot transcriptionally piggyback off neighboring conserved ORF (cannot share promoter  
362 with neighbor, *pink shading*) or can transcriptionally piggyback off neighboring conserved ORF  
363 (possible to share promoter with neighbor, *green shading*). D) Counts of *de novo* ORFs that are  
364 within 500 bp of a conserved ORF in different genomic orientations; ORFs further than 500bp  
365 are classified as independent. E) *De novo* ORFs in orientations that can piggyback have higher  
366 RNA expression levels than *de novo* ORFs in orientations that cannot piggyback (Cliff's Delta d  
367 = 0.4). Only *de novo* ORFs in a single orientation are considered (dashed box in panel D).  
368 Dashed line represents the median expression of independent *de novo* ORFs. F) *de novo* ORFs  
369 in orientations that can piggyback have higher coexpression with neighboring conserved ORFs  
370 compared to *de novo* ORFs in orientations that cannot piggyback (Cliff's Delta d = 0.43).  
371 Dashed line represents median coexpression of *de novo*-conserved ORF pairs on separate  
372 chromosomes. G) *de novo* ORFs in orientations that can piggyback are more likely to be  
373 transcriptionally associated with genes involved in the same biological processes as their  
374 neighboring conserved ORFs than *de novo* ORFs in orientations that cannot piggyback (Cliff's  
375 Delta d = 0.31). Dashed line represents median functional enrichment similarities of *de novo*-  
376 conserved ORF pairs on separate chromosomes. (For panels E-F-G: Mann-Whitney U-test, \*\*\*\*:  
377 p < 2.2e-16).

43

378

379 Previous literature has shown that many nORFs arise *de novo* from previously noncoding  
380 regions [24,26]. We wanted to investigate how these evolutionarily novel ORFs acquire  
381 expression and whether their locus of emergence influences this acquisition. To define which  
382 ORFs were of recent *de novo* evolutionary origins, we developed a multistep pipeline combining  
383 sequence similarity searches and syntenic alignments (Figure 4A). cORFs were considered  
384 conserved if they had homologues detectable by sequence similarity searches with BLAST in  
385 budding yeasts outside of the *Saccharomyces* genus or if their open reading frames were  
386 maintained within the *Saccharomyces* genus [14]. cORFs and nORFs were considered *de novo*  
387 if they lacked homologues detectable by sequence similarity outside of the *Saccharomyces*  
388 genus and if less than 60% of syntenic orthologous nucleotides in the two most distant  
389 *Saccharomyces* branches were in the same reading frame as in *S. cerevisiae*. These criteria  
390 aimed to identify the youngest *de novo* ORFs. Overall, we identified 5,624 conserved cORFs  
391 and 2,756 *de novo* ORFs including 77 *de novo* cORFs and 2,679 *de novo* nORFs (Figure 4B).  
392 In general, the coexpression patterns of *de novo* ORFs (Supplementary Figure 12) were similar  
393 to those of nORFs (Figure 3A-B).

394

395 We hypothesized that the locus where *de novo* ORFs arise may influence their expression  
396 profiles through “piggybacking” off their neighboring conserved ORFs’ pre-existing regulatory  
397 environment. To investigate this hypothesis, we categorized *de novo* ORFs based on their  
398 positioning relative to neighboring conserved ORFs. The *de novo* ORFs further than 500 bp  
399 from all conserved ORFs were classified as independent. The remaining *de novo* ORFs were  
400 classified as either upstream or downstream on the same strand (up same or down same),  
401 upstream or downstream on the opposite strand (up opposite or down opposite), or as  
402 overlapping on the opposite strand (anti-sense overlap) based on their orientation to the nearest  
403 conserved ORF (Figure 4C-D). We categorized the orientations as being able to piggyback or

44

22

45

404 unable to piggyback based on their potential of sharing a promoter with neighboring conserved  
405 ORFs, with down opposite and antisense overlap as orientations that cannot piggyback and up  
406 opposite, up same, and down same as orientations that can piggyback (Figure 4C). The  
407 piggybacking hypothesis predicts that *de novo* ORFs that arise in orientations that can  
408 piggyback would be positively influenced by the regulatory environment provided by the  
409 promoters of neighboring conserved ORFs, resulting in similar transcription profiles as their  
410 neighbors and increased expression relative to *de novo* ORFs that do not benefit from a pre-  
411 existing regulatory environment.

412

413 We considered three metrics to assess piggybacking: RNA expression level, measured as  
414 median TPM over all the samples analyzed, coexpression with neighboring conserved ORF and  
415 biological process similarity with neighboring conserved ORF. To calculate biological process  
416 similarity between two ORFs, we used significant GO terms at FDR < 0.01 determined by  
417 coexpression GSEA for each ORF (Supplementary Figure 10) and calculated the similarity  
418 between these two sets of GO terms using the relevance method [82]. If two ORFs are enriched  
419 in the same specialized terms, their relevance metric would be higher than if they are enriched  
420 in different terms or in the same generic terms. We found that *de novo* ORFs in orientations that  
421 can piggyback tend to have higher expression (focusing only on ORFs that could be assigned a  
422 single orientation, dashed box in Figure 4D, Cliff's Delta  $d = 0.4$ ; Figure 4E), higher  
423 coexpression with their neighbor (Cliff's Delta  $d = 0.43$ ; Figure 4F), and higher biological  
424 process similarity (Cliff's Delta  $d = 0.31$ ; Figure 4G), compared to ORFs in orientations that  
425 cannot piggyback ( $p < 2.2e-16$  Mann-Whitney U-test for all). Thus, all three metrics supported  
426 the piggybacking hypothesis.

427

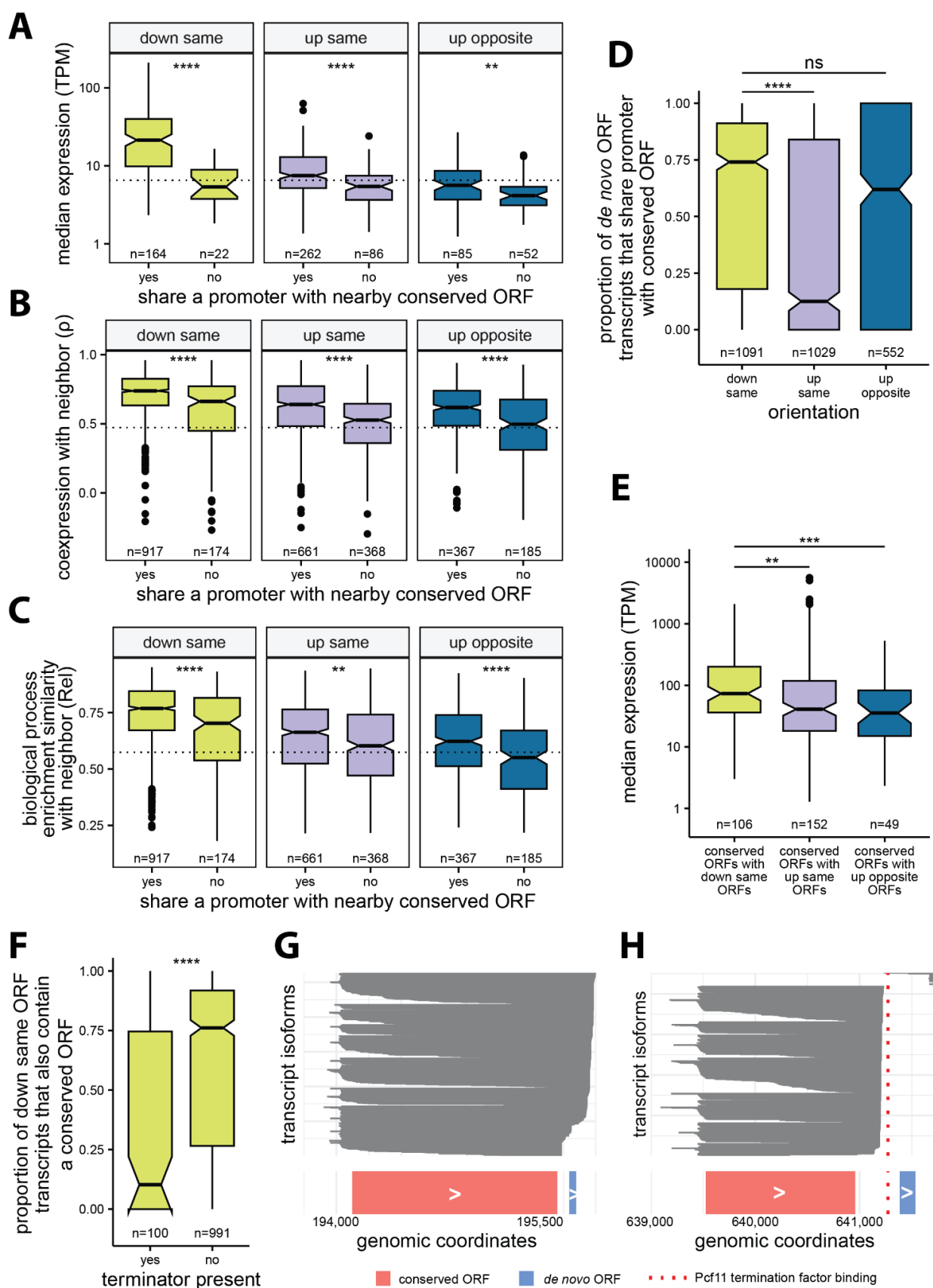
428 Closer examination revealed a more complex situation. First, the immediate neighbors of *de*  
429 *novo* ORFs in orientations that can piggyback were rarely among their strongest coexpression

47

430 partners (only found in the top 10 coexpressed partners for 15% of down same, 4.5% of up  
431 same, 3% of up opposite ORFs). Therefore, emergence nearby a conserved ORF in a  
432 piggybacking orientation influences, but does not fully determine, the transcription profiles of *de*  
433 *novo* ORFs. Transcriptional regulation beyond that provided by the pre-existing regulatory  
434 environment may exist. Second, while ORFs in all three orientations that can piggyback  
435 displayed increased coexpression and biological process similarity with their neighbors relative  
436 to background expectations (Supplementary Figure 13A-B), only down same *de novo* ORFs  
437 displayed increased RNA expression levels (Supplementary Figure 13C). The expression levels  
438 of up same *de novo* ORFs were statistically indistinguishable from independent *de novo* ORFs,  
439 while those of up opposite *de novo* ORFs were significantly lower than those of independent *de*  
440 *novo* ORFs (Supplementary Figure 13C). Down same *de novo* ORFs also showed stronger  
441 coexpression and biological process similarity with their conserved neighbors than up same and  
442 up opposite *de novo* ORFs (Supplementary figure 13A-B). Therefore, the transcription of down  
443 same *de novo* ORFs appeared most susceptible to piggybacking.

48

24



51

445 **Figure 5 Effects of promoter sharing on expression, coexpression and biological process**

446 **similarities of *de novo* ORFs**

447 A) *De novo* ORFs that share a promoter with neighboring conserved ORFs, as determined by  
448 TIF-seq transcript boundaries, have significantly higher expression levels than *de novo* ORFs  
449 that do not. Considering only ORFs in a single orientation. Dashed line represents the median  
450 expression of independent *de novo* ORFs. B) *De novo* ORFs that share a promoter with  
451 neighboring conserved ORFs have higher coexpression with their neighbors than *de novo*  
452 ORFs that do not share a promoter. Dashed line represents median coexpression of *de novo*-  
453 conserved ORF pairs on separate chromosomes. C) *De novo* ORFs that share a promoter have  
454 more similar functional enrichments with neighboring conserved ORFs than *de novo* ORFs that  
455 do not share a promoter. Dashed line represents median functional enrichment similarities of  
456 the background distribution of *de novo*-conserved ORF pairs on separate chromosomes. D)  
457 Down same *de novo* ORFs share a promoter with neighboring conserved ORFs significantly  
458 more often than up same ORFs. E) Conserved ORFs with downstream *de novo* ORFs have a  
459 significant increase in expression compared to conserved ORFs with upstream *de novo* ORFs.  
460 F) Existence of transcription termination factors (Pcf11 or Nrd1) in between conserved ORFs  
461 and nearby downstream *de novo* ORFs leads to less shared transcripts. G) Transcript isoforms  
462 (gray) at an example locus where there are no transcription termination factors present between  
463 conserved ORF YBL015W (*pink*) and downstream *de novo* ORF chr2:195794-195847(+) (*blue*).  
464 H) Transcript isoforms (gray) at an example locus where there is Pcf11 transcription terminator  
465 present (*red line*) between conserved ORF YPR034W (*pink*) and downstream *de novo* ORF  
466 chr16:641385-641534(+) (*blue*). All detected transcript isoforms on these loci are plotted for G  
467 and F. (For all panels: \*\*\*\*:  $p \leq 0.0001$ , \*\*\*:  $p \leq 0.001$ , \*\*:  $p \leq 0.01$ , \*:  $p \leq 0.05$ , ns: not-significant;  
468 Mann-Whitney U-test)

469

53

470 To understand the molecular mechanisms leading to the differences in expression,  
471 coexpression and biological process similarity between the orientations that can piggyback,  
472 which all have the potential to share a promoter with neighboring conserved ORF, we  
473 investigated which actually do by analyzing transcript architecture. Using a publicly available  
474 TIF-seq dataset [66], we defined down same or up same ORFs as sharing a promoter with their  
475 neighbor if they mapped to the same transcript at least once. We defined up opposite ORFs as  
476 sharing a promoter with their neighbor if their respective transcripts did not have overlapping  
477 TSSs, as would be expected for divergent promoters [83]. According to these criteria, 84% of  
478 down same ( $n = 174$ ), 64% of up same ( $n = 368$ ), and 66% of up opposite ( $n = 185$ ) *de novo*  
479 ORFs share a promoter with their neighboring conserved ORFs (Supplementary Figure 14).  
480 Among all *de novo* ORFs that arose in orientations that can piggyback, those that share  
481 promoters with neighboring conserved ORFs displayed higher expression levels than those that  
482 do not (*down same*:  $d = 0.75$ ,  $p = 1.06e-8$ ; *up same*:  $d = 0.38$ ,  $p = 1.23e-7$ ; *up opposite*:  $d = 0.3$ ,  
483  $p = 2.9e-3$  Mann-Whitney U-test,  $d$ : Cliff's Delta; Figure 5A). We also observed a significant  
484 increase in coexpression and biological process similarity between *de novo* ORFs and their  
485 neighboring conserved ORFs when their promoters are shared compared to when they are not  
486 (coexpression: *down same*:  $d = 0.28$ ,  $p = 2.99e-9$ ; *up same*:  $d = 0.31$ ,  $p < 2.2e-16$ ; *up opposite*:  
487  $d = 0.27$ ,  $p = 2.1e-7$ ; biological process similarity: *down same*:  $d = 0.24$ ,  $p = 5.5e-7$ ; *up same*:  $d$   
488  $= 0.108$ ,  $p = 3.78e-3$ ; *up opposite*:  $d = 0.24$ ,  $p = 6.1e-6$ ,  $d$ : Cliff's Delta, Mann-Whitney U-test;  
489 Figures 5B and 5C, respectively). Hence, sharing a promoter led to increases in the three  
490 piggybacking metrics for the three orientations.

491

492 Further supporting the notion that down same ORFs are particularly prone to piggybacking, the  
493 down same *de novo* ORFs that share a promoter with their conserved neighbors displayed  
494 much higher expression levels, and higher coexpression and biological process similarity with  
495 their conserved neighbor, than up same or up opposite ORFs that also share a promoter with

55

496 their conserved neighbors (expression: *down same vs up same*:  $d = 0.58$ ; *down same vs up*  
497 *opposite*:  $d = 0.55$ ; coexpression: *down same vs up same*:  $d = 0.29$ , *down same vs up opposite*:  
498  $d = 0.38$ ; biological process similarity: *down same vs up same*:  $d = 0.37$ , *down same vs up*  
499 *opposite*:  $d = 0.45$ ;  $d$ : Cliff's Delta,  $p < 2.2e-16$  for all comparisons, Mann-Whitney U-test). This  
500 could be due to down same ORF's tendency to share promoters more often than up same  
501 ORFs, as a larger proportion of transcripts containing down same ORFs also contain a  
502 conserved ORF (*down same vs up same*: Cliff's Delta  $d = 0.26$ , Mann-Whitney U-test  $p < 2.2e-$   
503 16; Figure 5D), or higher expression levels of conserved ORFs that have down same ORFs on  
504 their transcripts compared to conserved ORFs with up same or up opposite piggybacking ORFs  
505 (*down same vs up same*:  $d = 0.2$ ,  $p = 5.4e-3$ ; *down same vs up opposite*:  $d = 0.34$ ,  $p = 6.5e-4$ ,  
506 Mann-Whitney U-test,  $d$ : Cliff's Delta; Figure 5E).

507

508 Based on these results, we reasoned that transcriptional readthrough could be the molecular  
509 mechanism underlying the efficient transcriptional piggybacking of down same *de novo* ORFs.  
510 To investigate this hypothesis, we examined the impact of transcription terminators Pcf11 or  
511 Nrd1 on the frequency of transcript sharing between a conserved ORF and its downstream *de*  
512 *novo* ORF. Analyzing publicly available ChIP-exo data [65], we found that the presence of  
513 terminators between conserved ORFs and their downstream *de novo* ORF pairs resulted in a  
514 notably lower percentage of shared transcripts (Cliff's Delta  $d = -0.39$ ,  $p = 1.59e-10$ , Mann-  
515 Whitney U-test; Figure 5F). As an illustration, consider the genomic region on chromosome II  
516 from bases 194,000 to 196,000, containing the conserved ORF YBL015W and a downstream  
517 *de novo* ORF (positions 195,794 to 195,847). No terminator factor is bound to the intervening  
518 DNA between these two ORFs. This pair has high coexpression, with  $p = 0.96$  and we observed  
519 that nearly all transcripts in this region containing the *de novo* ORF also include YBL015W  
520 (Figure 5G). In contrast, the genomic region on chromosome XVI from 639,000 to 641,800,  
521 containing the conserved ORF YPR034W and downstream *de novo* ORF (positions 641,385 to

57

522 641,534), does have a Pcf11 terminator factor between the pair, and as expected, none of the  
523 transcripts in this region contain both YPR034W and the *de novo* ORF, which have poor  
524 coexpression as a result ( $\rho = 0.1$ ; Figure 5H). We conclude that sharing a transcript via  
525 transcriptional readthrough is the major transcriptional piggybacking mechanism for down same  
526 *de novo* ORFs.

## 527 Discussion

528 We explored the transcription of nORFs from multiple angles including network topology,  
529 associations with cellular processes, TF regulation, and influence of the locus of emergence on  
530 *de novo* ORF expression. Delving into network topology, we find that nORFs have distinct  
531 expression profiles that are strongly correlated with only a few other ORFs. Nearly all cORFs  
532 are coexpressed with at least one nORF, but the converse is not true. Numerous nORFs form  
533 new structured transcriptional modules, possibly involved in both known and unknown cellular  
534 processes. The addition of nORFs to the cellular network resulted in a more clustered network  
535 than expected by chance, highlighting the previously unsuspected influence of nORFs in  
536 shaping the coexpression landscape.

537

538 Our study is the first to show a large-scale association between the expression of nORFs and  
539 cellular homeostasis and transport processes. We anticipate that future studies will follow up to  
540 test these associations experimentally. We also found nORFs to be preferentially associated  
541 with cellular processes related to metabolism, transposition and cell adhesion, but rarely with  
542 the core processes of the central dogma, DNA, RNA or protein processing. Genes involved in  
543 transport, metabolism, and stress tend to have more variable expression compared to genes in  
544 other pathways [84]. Pathways with more variable expression could be more likely to

59

545 incorporate novel ORFs, possibly as a form of adaptive transcriptional response. There are  
546 several consistent observations in the literature [47,85,86]. For instance, Li et al. [47] showed  
547 that many *de novo* ORFs are upregulated in heat shock. Wilson and Masel [87] found higher  
548 translation of *de novo* ORFs under starvation conditions. Carvunis et al. [24] found *de novo*  
549 cORFs are enriched for the GO term 'response to stress'. Other studies showed examples of  
550 how specific *de novo* ORFs could be involved in stress response [35,88] or homeostasis  
551 [88,89]. For instance the *de novo* antifreeze glycoprotein AFGP allows Arctic codfish to live in  
552 colder environments [35] or *MDF1* in yeast [88,90] was found in a screen to provide resistance  
553 to certain toxins and mediates ion homeostasis [91]. Our results, combined with these previous  
554 investigations, argue that a large fraction of nORFs provide adaptation to stresses and help  
555 maintain homeostasis, perhaps through modulation of transport processes.

556

557 Recent research in yeast has revealed an enrichment of transmembrane domains [15,24,92,93]  
558 within *de novo* ORFs. Previous studies identified small nORFs and *de novo* ORFs that localize  
559 to diverse cellular membranes, such as those of the endoplasmic reticulum, Golgi, or  
560 mitochondria in different species [10,15,94–97]. These findings are consistent with the notion  
561 that *de novo* ORFs could play a role in a range of transport processes, such as ion, amino acid,  
562 or protein transport across cellular membranes. By establishing a connection between predicted  
563 transmembrane domains and increased coexpression with transport-related genes, our findings  
564 set the stage for future experimental investigations into the precise molecular mechanisms and  
565 functional roles of nORFs in diverse transport systems.

566

567 Lastly, we explored how the preexisting regulatory context influences the transcriptional profiles  
568 of *de novo* ORFs. We found that *de novo* ORFs that piggyback off their neighboring conserved

61

569 ORFs' promoters had increases in expression, coexpression and biological process similarity  
570 with their neighboring conserved ORFs. Strikingly, ORFs that emerge *de novo* downstream of  
571 conserved ORFs have the largest increases in expression, coexpression and biological process  
572 similarities with their neighbors compared to other orientations, largely due to transcriptional  
573 readthrough leading to transcript sharing. Previous studies have shown that the transcription of  
574 regions downstream of genes is functional and regulated [98]. A study in humans showed that  
575 readthrough transcription downstream of some genes is responsible for roughly 15%–30% of  
576 intergenic transcription and is induced by osmotic and heat stress creating extended transcripts  
577 that play a role in maintaining nuclear stability during stress [99]. Another study in humans and  
578 zebrafish showed that the translation of small ORFs located in the 3' UTR of mRNAs (dORFs)  
579 increased the translation rate of the upstream gene [100]. Lastly, a study in yeast found that  
580 genes which are preferentially expressed as bicistronic transcripts tend to contain evolutionarily  
581 younger genes compared to adjacent genes that do not share transcripts, suggesting that  
582 transcript sharing could provide a route for novel ORFs to become established genes [101].  
583 These findings together with our results suggest that genomic regions downstream of genes  
584 may provide the most favorable environment for the transcription of *de novo* ORFs.

585

586 Our analyses show that the likelihood of a *de novo* ORF being expressed or repressed under  
587 the same conditions as the neighboring conserved ORF is influenced by the extent to which it  
588 piggybacks on the neighboring ORF's regulatory context. Therefore, in addition to the  
589 evolutionary pressure acting on the sequence of emerging ORFs, our results suggest that  
590 transcriptional regulation and genomic context also influence their functional potential. However,  
591 this influence is not entirely deterministic, and much weaker when *de novo* ORFs emerge  
592 upstream than downstream of genes. Future studies are needed to map regulatory networks  
593 controlling nORF expression and reconstruct their evolutionary histories.

63

594

595 There are several limitations to our study. First, while SpQN enhances the coexpression signal  
596 of lowly expressed ORFs, it comes at the cost of reducing signals in highly expressed ORFs  
597 [62]. Given our objective of studying lowly-expressed nORFs this tradeoff is deemed worthwhile.  
598 Second, our study provides evidence of associations between nORFs and cellular processes  
599 such as homeostasis and transport, but these findings are based on transcription profile  
600 similarities which do not necessarily imply cotranslation or correlated protein abundances [102].  
601 Furthermore, our analyses were performed in the yeast *S. cerevisiae* and the generalizability of  
602 our findings to other species requires further investigation.

## 603 Conclusions

604 In conclusion, our study represents a significant step forward towards the characterization of  
605 nORFs. We employed advanced statistical methods to account for low expression levels and  
606 generate a high-quality coexpression network. Despite being lowly expressed, nORFs are  
607 coexpressed with almost every cORF. We find that numerous nORFs form structured,  
608 noncanonical-only transcriptional modules which could be involved in regulating novel cellular  
609 processes. We find that many nORFs are coexpressed with genes involved in homeostasis and  
610 transport related processes, suggesting that these pathways are most likely to incorporate novel  
611 ORFs. Additionally, our investigation into the influence of genomic orientation on the expression  
612 and coexpression of *de novo* ORFs showed that ORFs located downstream of conserved ORFs  
613 are most influenced by the pre-existing regulatory environment at their locus of emergence. Our  
614 findings provide a foundation for future research to further elucidate the roles of nORFs and *de*  
615 *novo* ORFs in cellular processes and their broader implications in adaptation and evolution.

65

## 616 Methods

### 617 Creating ORF list

618 To create our initial ORF list, we utilized two sources. First, we took annotated ORFs in the *S.*  
619 *cerevisiae* genome R64-2-1 downloaded from SGD [103], which included 6,600 ORFs. Second,  
620 we utilized the translated ORF list from Wacholder et al. [14] reported in their *Supplementary*  
621 *Table 3*. We filtered to include cORFs (Verified, Uncharacterized or Transposable element  
622 genes) as well as any nORFs with evidence of translation at *q* value < 0.05 (Dubious,  
623 Pseudogenes and unannotated ORFs). We removed ORFs with lengths shorter than the  
624 alignment index kmer size of 25nt used for RNA-seq alignment. In situations where ORFs  
625 overlapped on the same strand with greater than 75% overlap of either ORF, we removed the  
626 shorter ORF using bedtools [104]. We removed ORFs that were exact sequence duplicates of  
627 another ORF. This left 5,878 cORFs and 18,636 nORFs, for a total of 24,514 ORFs used for  
628 RNA-seq alignment.

### 629 RNA-seq data preprocessing

630 Strand specific RNA-seq samples were obtained from the Sequencing Read Archive (SRA)  
631 using the search query (*saccharomyces cerevisiae*[Organism]) AND *rna sequencing*. Each  
632 study was manually inspected and only studies that had an accompanying paper or detailed  
633 methods on Gene Expression Omnibus (GEO) were included. Samples were quality controlled  
634 (nucleotides with Phred score < 20 at end of reads were trimmed) and adapters were removed  
635 using TrimGalore version 0.6.4 [105]. Samples were aligned to the transcriptome GTF file  
636 containing the ORFs defined above and quantified using Salmon [106] version 0.12.0 with an  
637 index kmer size of 25. Samples with less than 1 million reads mapped or unstranded samples

67

638 were removed, resulting in an expression dataset of 3,916 samples from 174 studies  
639 (Supplementary Data 1). ORFs were removed to limit sparsity and increase the number of  
640 observations in the subsequent pairwise coexpression analysis. Only ORFs that had at least  
641 400 samples with a raw count > 5 were included for downstream coexpression analysis, n =  
642 11,630 ORFs (5,803 canonical and 5,827 noncanonical, Supplementary Data 2).

## 643 Coexpression calculations

644 The raw counts were transformed using clr. Pairwise proportionality was calculated using  $\rho$  [69]  
645 for each ORF pair. Spatial quantile normalization (SpQN) [62] of the coexpression network was  
646 performed using the mean clr expression value for each ORF as confounders to correct for  
647 mean expression bias, which resulted in similar distributions of coexpression values across  
648 varying expression levels (Supplementary Figure 2). Only ORF pairs that had at least 400  
649 samples expressing both ORFs (at raw >5) were included. This threshold was determined  
650 empirically as detailed below.

651

652 Since zero values cannot be used with log ratio transformations, all zeros must be removed  
653 from the dataset. Proposed solutions in the literature on how to remove zeros, all of which have  
654 their pros and cons, include removing all genes that contain any zeros, imputing the zeros, or  
655 adding a pseudo count to all genes [107,108]. Removing all ORFs that contain any zeros is not  
656 possible for this analysis since the ORFs of interest are lowly and conditionally expressed. The  
657 addition of pseudocounts can be problematic when dealing with lowly expressed ORFs, for the  
658 addition of a small count is much more substantial for an ORF with a low read count compared  
659 to an ORF with a high read count [109]. For these reasons, all raw counts below 5 were set to  
660 NA prior to clr transformation. These observations were then excluded when calculating the clr

69

661 transformation and in the  $\rho$  calculations. We used clr and  $\rho$  implementations in R package *Propr*  
662 [69] and implementation of SpQN from Wang et al. [62].

663

664 To determine the minimum number of samples needed expressing both ORFs in a pair, we  
665 determined the number of samples needed for coexpression values to converge within  $\rho \pm 0.05$   
666 or  $\rho \pm 0.1$  for 2,167 nORF-cORF pairs which have a  $\rho > 99$ th percentile (before SpQN). All  
667 samples expressing both ORFs in a pair were randomly binned into groups of 10, and  $\rho$  was  
668 calculated after each addition of another sample. Fluctuations were calculated as  $\max(\rho) - \min(\rho)$   
669 within a sample bin. Convergence was determined as the first sample bin with fluctuations  $\leq$   
670 fluctuation threshold, either 0.05 or 0.01 (Supplementary Figure 1).

## 671 Comparing coexpression inference approaches

672 To compare our approach with a batch correction approach, we used clr to transform the  
673 expression matrix, followed by removing the top principal component (PC1) of the clr expression  
674 matrix to do batch correction using the function *removePrincipalComponents* from the *WGCNA*  
675 [70] R package. We then calculated  $\rho$  values and applied SpQN normalization. Additionally, we  
676 created a coexpression matrix based on TPM as well as RPKM normalized expression values  
677 instead of clr and calculated Pearson's correlation coefficient.

## 678 Protein Complex enrichments

679 We retrieved a manually curated list of 408 protein complexes in *S. cerevisiae* from the  
680 CYC2008 database by Pu et al. [64]. The coexpression matrix was filtered to contain only the  
681 1,617 cORFs found in the CYC2008 database prior to creating the contingency table. Fisher's  
682 exact test was used to calculate the significance of the association between coexpression and

71

683 protein complex formation. Coexpressed was defined as the 99.8th  $\rho$  percentile ( $\rho > 0.888$ )  
684 considering all ORF pairs in the coexpression matrix ( $n = 62,204,406$  ORF pairs) for Figure 1C.

## 685 TF binding enrichments

686 A ChIP-exo dataset from Rossi et al. [65] containing DNA-binding information for 73 sequence-  
687 specific TFs across the whole genome was used. For each ORF we identified which TFs had  
688 binding within 200 bp upstream of the ORF's TSS. The TSSs for all ORFs in the coexpression  
689 matrix was determined by the median 5' transcript isoform (TIF) start positions using TIF-seq  
690 [66] dataset. Only ORFs found in the TIF-seq dataset were considered ( $n = 5,334$  cORFs and  
691 5,362 nORFs). To calculate the enrichments reported in Figures 1D, Supplementary Figure 5  
692 and Supplementary Figure 7, the coexpression matrix was first filtered to only include ORFs that  
693 have at least 1 TF binding within 200 bp upstream of its TSS ( $n = 973$  cORFs and 936 nORFs).  
694 Fisher's exact test was used to calculate the association between coexpression and having their  
695 promoters bound by a common TF. Coexpressed was defined as the 99.8th  $\rho$  percentile ( $\rho >$   
696 0.888) considering all ORF pairs in the coexpression matrix ( $n = 62,204,406$  ORF pairs) for  
697 Figure 1D.

## 698 Coexpression matrix clustering

699 We used the weighted gene coexpression network analysis (WGCNA) package [70] in R to  
700 cluster our coexpression matrix. To do this, we first transformed our coexpression matrix into a  
701 weighted adjacency matrix by applying a soft thresholding which involved raising the  
702 coexpression matrix to the power of 12. This removed weak coexpression relationships from the  
703 matrix. We then used the topological overlap matrix (TOM) similarity to calculate the distances  
704 between each column and row of the matrix. Using the *hclust* function in R with the *ward*  
705 clustering method, we created a hierarchical clustering dendrogram. We then used the dynamic

73

706 tree cutting method within the *WGCNA* package to assign ORFs to coexpression clusters,  
707 resulting in 73 clusters of which 69 were mapped to the full coexpression network. ORFs in the  
708 other four clusters were not included in the network as they did not pass the  $\rho$  threshold.

## 709 GO analysis of clusters

710 We downloaded GO trees (file: go-basic.obo) and annotations (files: sgd.gaf) from ref. [110]. We  
711 used the Python package, *GOATools* [111], to calculate the number of genes associated with  
712 each GO term in a cluster and the overall population of (all) genes in the coexpression matrix.  
713 We excluded annotations based on the evidence codes ND (no biological data available). We  
714 identified GO term enrichments by calculating the likelihood of the ratio of the cORFs associated  
715 with a GO term within a cluster given the total number of cORFs associated with the same GO  
716 term in the background set of all cORFs in the coexpression matrix. We applied Fisher's exact  
717 test and FDR with BH multiple testing correction [112] to calculate corrected p-values for the  
718 enrichment of GO term in the clusters. FDR  $< 0.05$  was taken as a requirement for significance.  
719 We applied GO enrichment calculations only when there were at least 5 cORFs in the cluster  
720 (n=54).

## 721 Network randomization and topology analyses

722 To create random networks while preserving the same degree distribution, we used an edge  
723 swapping method (Supplementary Figure 9). This involved randomly selecting two edges in the  
724 network, which were either cORF-nORF or nORF-nORF edges and swapping them. The swap  
725 was accepted only if it did not disconnect any nodes from the network and the newly generated  
726 edges were not already present in the network. We repeated this process for at least ten times  
727 the number of edges in the network. Network diameter and transitivity were calculated using R

75

728 package *igraph* [113] and networks were plotted using spring embedded layout [74] in Python  
729 package *networkx* [114].

## 730 Gene set enrichment analysis

731 Gene set enrichment analysis (GSEA) calculates enrichments of an ordered list of genes given  
732 a biological annotation such as GO or KEGG. For each ORF in our dataset, we used p values to  
733 order annotated ORFs and provided this sorted set to *fgsea* [115]. We used the GO slim file  
734 downloaded from SGD [103] for GO annotations. We used *clusterProfiler* [116] R package to  
735 download KEGG annotations using KEGG REST API [78] on 1 April 2023 and then used  
736 *fgseaMultilevel* function in *fgsea* R package to calculate enrichments for both annotations  
737 individually. To calculate GO or KEGG terms that are enriched or depleted for nORFs compared  
738 to cORFs, we calculated the number of cORFs and nORFs that had GSEA enrichments at BH  
739 adjusted FDR < 0.01. Using these counts we calculated the proportion of nORFs and cORFs  
740 associated with a GO or KEGG term and used Fisher's exact test to assess the significance of  
741 association. P values returned by Fisher's exact test were corrected for multiple hypothesis  
742 testing using BH correction. Odds ratios were calculated by dividing proportion of nORFs to  
743 proportion of cORFs. Proportions for the GO terms with BH adjusted FDR < 0.001 and Odds  
744 ratio greater than 2 or less than 0.5 are plotted in Figures 3A-B and are reported in  
745 Supplementary Data 5 and proportions for KEGG terms are plotted in Supplementary Figure 11  
746 and reported in Supplementary Data 6.

## 747 Transmembrane domain enrichment

748 Transmembrane domains were predicted using TMHMM 2.0 [75] for all nORFs. An ORF was  
749 classified as having a transmembrane domain if it was predicted to have at least one  
750 transmembrane domain. nORFs were classified as "coexpressed with transport-related genes" if

77

751 the ORF had a GSEA enrichment at FDR < 0.01 with any of the 15 GO slim transport terms:  
752 transport, ion transport, amino acid transport, lipid transport, carbohydrate transport, regulation  
753 of transport, transmembrane transport, vacuolar transport, vesicle-mediated transport,  
754 endosomal transport, nucleobase-containing compound transport, Golgi vesicle transport,  
755 nucleocytoplasmic transport, nuclear transport, or cytoskeleton-dependent intracellular  
756 transport. Fisher's exact test was used to calculate the significance of association between  
757 transport-related processes and transmembrane domain.

758 **Differential expression analysis for TF deletion and  
759 overrepresentation tests**

760 For Hsf1 analysis, RNA-seq samples were from Ciccarelli et al. (SRA accession SRP437124)  
761 [76]. Hsf1 deletion strains were compared to wild type (WT) strains when exposed to heat shock  
762 conditions. For Sfp1 analysis, RNA-seq samples were from SRA accession SRP159150. In both  
763 cases, deletion strains were compared to WT strains. Differential expression was calculated  
764 using R package *DESeq2* [117], and ORFs were defined as differentially expressed if the log  
765 fold change (FC) in RNA expression between WT and control strains was greater than or less  
766 than 0.5 i.e.  $\log(\text{FC}) > 0.5$  or  $\log(\text{FC}) < -0.5$  and BH adjusted p-value < 0.05. ChIP-exo data for  
767 Hsf1 and Sfp1 binding was taken from Rossi et al. [65] and an ORF was labeled as having Hsf1  
768 or Sfp1 binding if the TF was found within 200 bp upstream of the ORF's TSS. Fisher's exact  
769 test was performed to see if there is an association between an nORF in a GO biological  
770 process and being regulated by the TF. We define an nORF to be "in" a GO term if it has a  
771 GSEA enrichment for that GO term at FDR < 0.01. We defined an nORF as regulated by a TF if  
772 the nORF had evidence of the TF binding within 200 bp of the nORF's TSS in ChIP-exo and has  
773 significantly downregulated expression in the TF deletion RNA-seq samples compared to the

79

774 WT samples. BH p-value correction was performed for all GO terms tested. Significant GO  
775 terms and the associated regulated nORFs are reported in Supplementary Data 8.

## 776 Detection of homologs using BLAST

777 We obtained the genomes of 332 budding yeasts from Shen et al. [118]. To investigate the  
778 homology of each non overlapping ORF in our dataset, we used TBLASTN and BLASTP [119]  
779 against each genome in the dataset, excluding the *Saccharomyces* genus. Default settings  
780 were used, with an e-value threshold of 0.0001. The BLASTP analysis was run against the list  
781 of protein coding genes used in Shen et al., while the TBLASTN analysis was run against each  
782 entire genome. We also applied BLASTP to annotated ORFs within the *S. cerevisiae* genome to  
783 identify homology that could be caused by whole genome duplication or transposons.

## 784 Identification of *de novo* and conserved ORFs

785 To identify *de novo* ORFs, we applied several strict criteria. Firstly, we obtained translation q-  
786 values and reading frame conservation (RFC) data from Wacholder et al. [14]. All cORFs and  
787 only nORFs with a translation q-value less than 0.05 were considered as potential *de novo*  
788 candidates. We excluded ORFs that overlapped with another cORF on the same strand or had  
789 TBLASTN or BLASTP hits outside of the *Saccharomyces* genus at e-value < 0.0001. Moreover,  
790 we eliminated ORFs that had BLASTP hits to another cORF in *S. cerevisiae*. From the  
791 remaining list of candidate *de novo* ORFs, we investigated whether their ancestral sequence  
792 could be noncoding. To do this, we utilized RFC values for each species within *Saccharomyces*  
793 genus. We classified ORFs as *de novo* if the RFC values for the most distant two branches  
794 were less than 0.6, suggesting the absence of a homologous ORF in those two species.  
795 We identified conserved ORFs if a nonoverlapping cORF has an average RFC > 0.8 or has  
796 either TBLASTN or BLASTP hit at e-value < 0.0001 threshold.

81

797 To identify conserved cORFs with overlaps we first considered if the cORFs had a BLASTP  
798 outside of *Saccharomyces* genus with e-value < 0.0001. Then for two overlapping ORFs, if one  
799 had RFC > 0.8 and the other had RFC < 0.8, we considered the one with higher RFC as  
800 conserved. For the ORF pairs that were not assigned as conserved using these two criteria, we  
801 applied TBLASTN for the non-overlapping parts of the overlapping pairs. Those with a  
802 TBLASTN hit with e-value < 0.0001 were considered conserved. We found a total of 5,624  
803 conserved ORFs and 2,756 *de novo* ORFs.

## 804 Calculation of GO term similarities

805 GO term similarities were calculated using the Relevance method developed in Schlicker et al.  
806 [82]. This method considers both the information content (IC) of the GO terms that are being  
807 compared and the IC of their most informative ancestor. IC represents the frequency of a GO  
808 term; thus, an ancestral GO term has lower IC than a descendant. We used the *GOSemSim*  
809 [120] package in R that implements these similarity measures.

83

## 810 Termination factor binding analysis

811 ChIP-exo data for Pcf11 and Nrd1 termination factor binding sites are taken from Rossi et al.  
812 [65]. This study reports binding sites at base pair resolution for *S. cerevisiae* for around 400  
813 proteins. We used supplementary bed formatted files for Pcf11 and Nrd1, which are known  
814 transcriptional terminators, and used in house R scripts to find binding sites within the regions  
815 between the stop codon of conserved ORFs and the start codon of down same *de novo* ORFs.  
816 ORF pairs were classified as having terminators present between them if there was either Pcf11  
817 or Nrd1 binding.

## 818 Determining shared promoters

819 To determine whether two ORFs shared a promoter, we reused the TIF-Seq dataset from  
820 Pelechano et al. [66]. TIF-Seq is a sequencing method that detects the boundaries of TIFs. We  
821 extracted all reported TIFs from the supplementary data file S1 and identified all TIFs that fully  
822 cover each ORF in both YPD and galactose. We then used this information to find ORF pairs  
823 that mapped to the same TIFs for down same and up same pairs, as well as found TIFs with  
824 non-overlapping TSSs for up opposite *de novo*-conserved ORF pairs. ORF pairs where the  
825 conserved ORF was not found in the TIF-seq dataset were not included and pairs where the *de*  
826 *novo* ORF was not found were considered to not share a promoter.

## 827 Web application

828 We utilized R language [121] and the shiny framework [73] to develop a web application which  
829 allows querying of ORFs in our dataset for information about their coexpression with other  
830 ORFs, network visualization, and GSEA enrichments. It can be accessed through a web  
831 browser and is available at <https://carvunislab.csb.pitt.edu/shiny/coexpression/>.

84

42

85

## 832 Acknowledgments

833 Figures 1A, 4A, 4C, and Supplementary Figure 10 were created with BioRender.com. The  
834 authors are grateful to Dr. Aaron Wacholder, Carly Houghton, Nelson Coelho, Dr. Saurin Bipin  
835 Parikh, Jiwon Lee, Lin Chou, Alistair Turcan, Dr. Nikolaos Vakirlis, and Dr. Maria Chikina for  
836 reviewing the manuscript prior to submission.

## 837 Author Contributions

838 Conceptualization: A.R., O.A., and A.-R.C.; Methodology: A.R, O.A.; Investigation: A.R, O.A.;  
839 Writing-original draft: A.R, O.A.; Writing-review and editing: A.R., O.A., and A.-R.C.;  
840 Supervision: A.-R.C. All authors approved the final version of the manuscript.

## 841 Funding

842 This work was supported by: the National Science Foundation under Grant No. 2144349  
843 awarded to A.-R.C and the National Science Foundation Graduate Research Fellowship under  
844 Grant No. 2139321 awarded to A.R. The funders had no role in study design, data collection  
845 and analysis, decision to publish, or preparation of the manuscript.

## 846 Source code

847 All source codes for the analyses conducted are accessible online at  
848 [https://www.github.com/oacar/noncanonical\\_coexpression\\_network](https://www.github.com/oacar/noncanonical_coexpression_network)

87

## 849 Ethics Declarations

### 850 Ethics approval and consent to participate

851 Not applicable.

### 852 Consent for publication

853 Not applicable.

### 854 Competing interests

855 A.-R.C. is a member of the scientific advisory board for ProFound Therapeutics (Flagship Labs

856 69, Inc).

## 857 Supplementary Data

858 Supplementary data files are available on Figshare

859 <https://doi.org/10.6084/m9.figshare.22289614>

860 **Supplementary Data 1:** RNA-seq studies and samples used in this study. (CSV)

861 **Supplementary Data 2:** ORFs included in the coexpression matrix. (CSV)

862 **Supplementary Data 3:** Coexpression matrix generated in this study. (CSV)

863 **Supplementary Data 4:** GSEA analysis results for each ORF using GO BP annotations. (CSV)

89

864 **Supplementary Data 5:** List of GO BP terms that are more associated with nORFs than cORFs  
865 and statistics. (CSV)

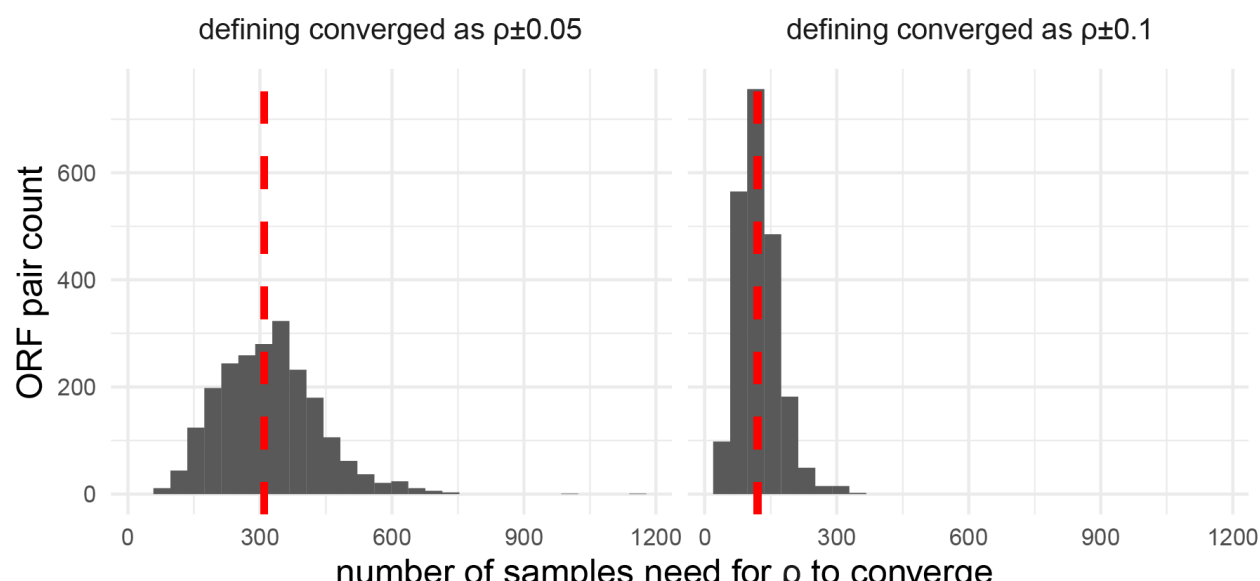
866 **Supplementary Data 6:** List of KEGG terms that are more associated with nORFs than cORFs  
867 and statistics. (CSV)

868 **Supplementary Data 7:** GSEA analysis results for each ORF using KEGG annotations. (CSV)

869 **Supplementary Data 8:** GO BP terms where nORFs are regulated by either Hsf1 or Sfp1 in GO  
870 BP terms are overrepresented. (CSV)

## 871 Supplementary Figures

### 872 Supplementary Figure 1



873

874 Supplementary Figure 1 To understand the effect of sample size on coexpression values and to  
875 determine how many samples is sufficient for  $p$  to converge, we recalculated coexpression for a  
876 given ORF pair using  $n = 2$  samples through  $n = \text{all samples}$ . Fluctuations were calculated as

91

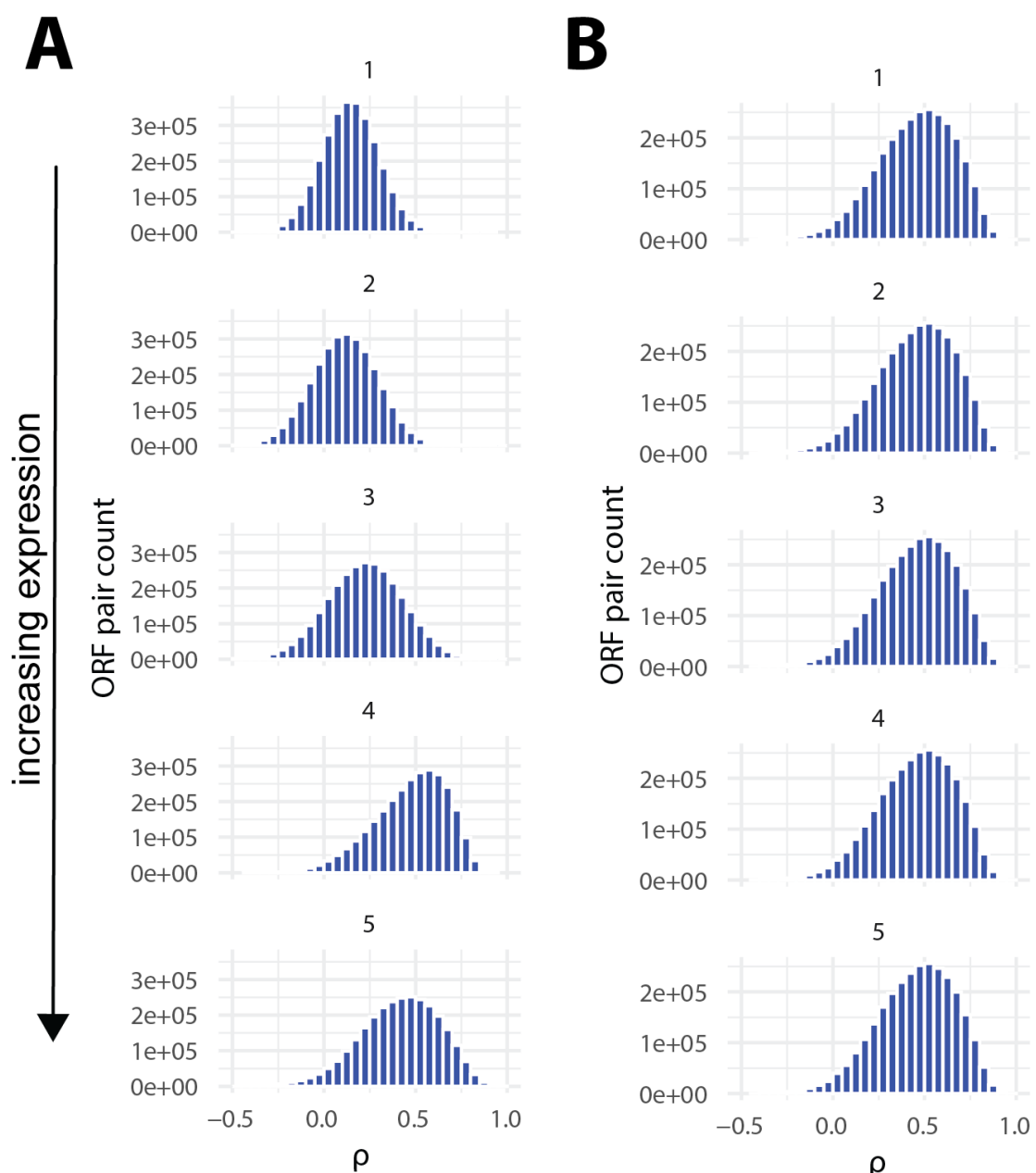
877  $\max(\rho) - \min(\rho)$  within bins of 10 samples. The number of samples needed for  $\rho$  to converge was  
878 calculated as the first sample bin where  $\rho$  fluctuations  $\leq$  fluctuation threshold, either 0.1 or 0.05.  
879 Histogram showing the minimum number of samples needed for  $\rho$  values to converge within  $\rho \pm$   
880 0.05 (*left*) and  $\rho \pm 0.1$  (*right*) for 2,167 cORF-nORF pairs with  $\rho >$  99th percentile. Red dashed  
881 lines show the median number of samples needed.

92

46

93

882 Supplementary Figure 2

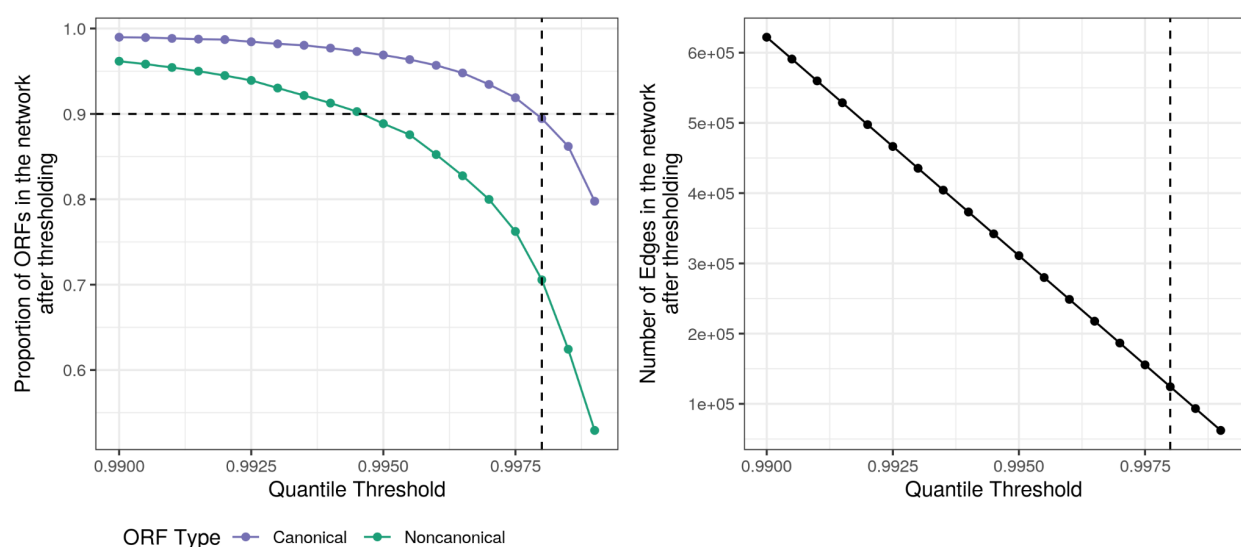


883

884 Supplementary Figure 2 Distribution of coexpression values ( $\rho$ ) for ORF pairs binned by  
885 expression level, from lowly expressed pairs *top* to highly expressed pairs *bottom*, A) before  
886 spatial quantile normalization (SpQN) and B) after SpQN, which normalizes the coexpression  
887 values so that the distribution within each expression bin is similar.

95

888 Supplementary Figure 3



889 ORF Type —●— Canonical —●— Noncanonical

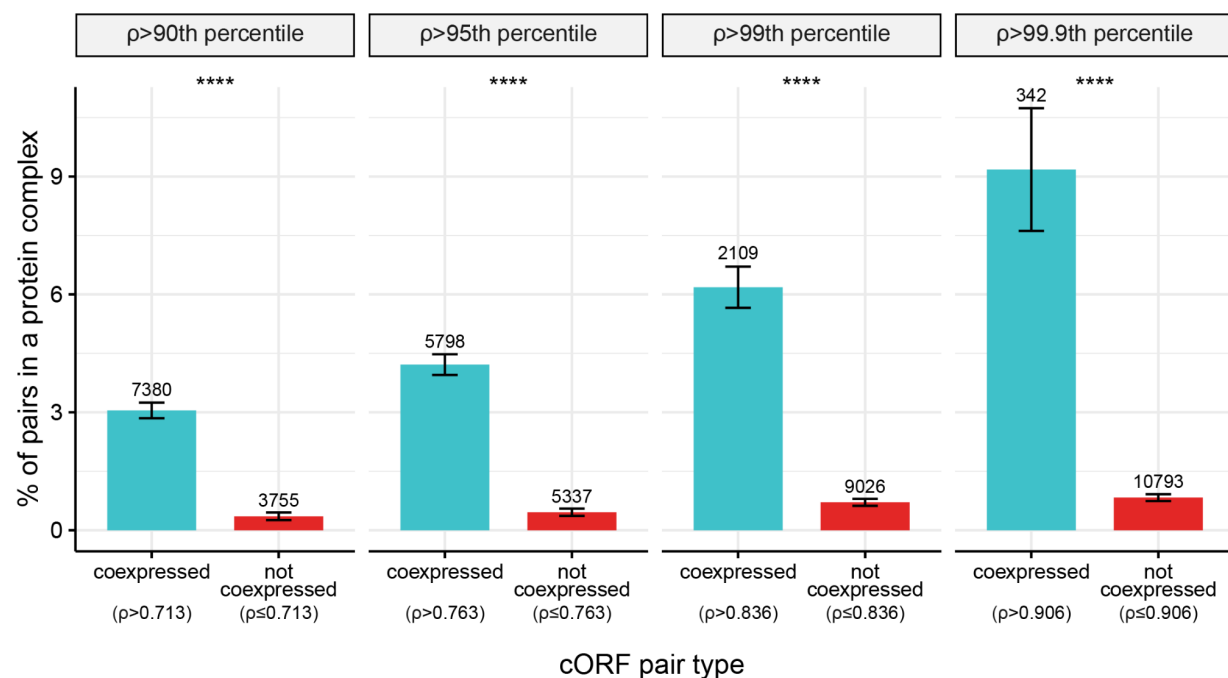
890 Supplementary Figure 3 Network threshold affects cORFs and nORFs differently. *Left* shows  
891 the proportion of cORFs or nORFs in the network at each quantile threshold and the *right* shows  
892 the number of connections in the network. Dashed line represents 0.9998 quantile which was  
893 chosen for creating the network.

96

48

97

894 Supplementary Figure 4



895

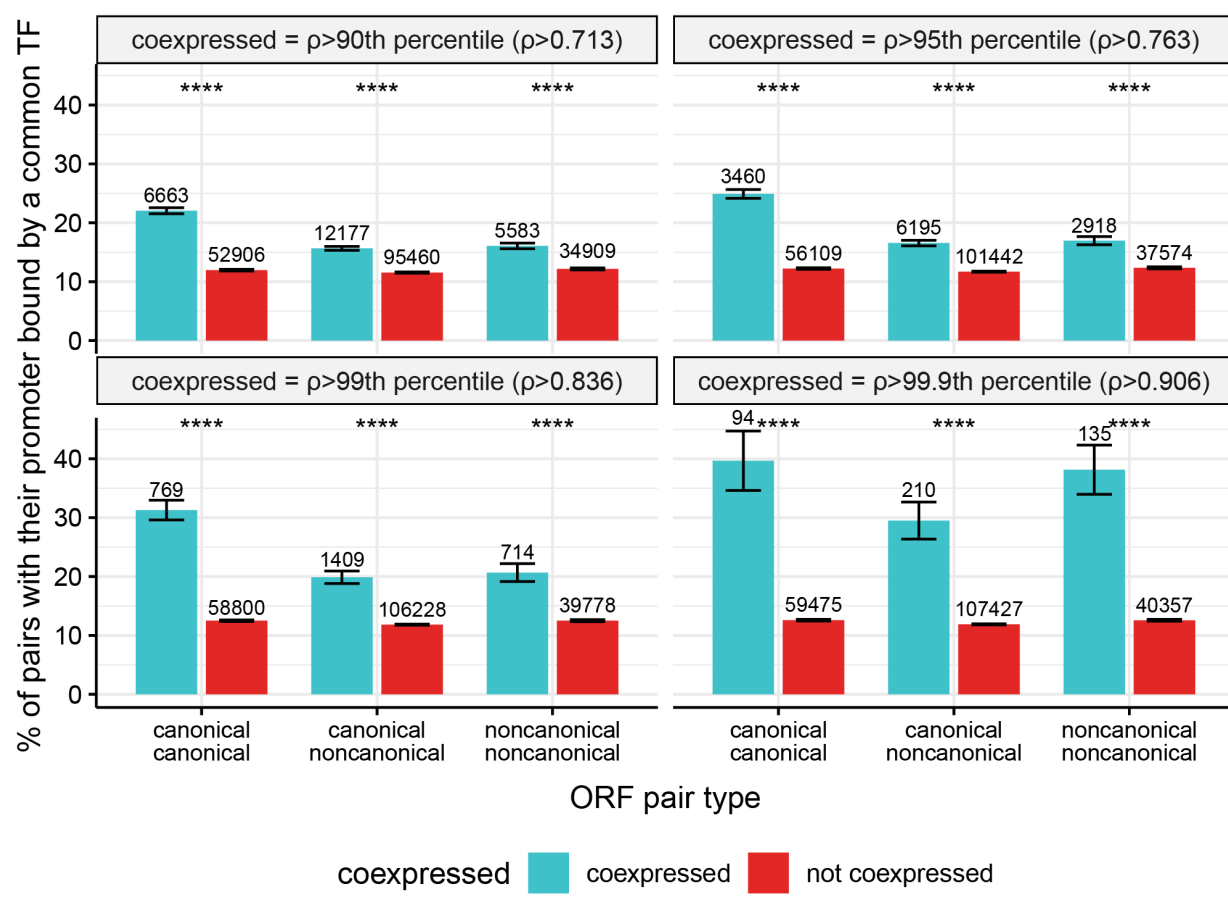
896 Supplementary Figure 4 Coexpressed cORFs pairs are more likely to encode proteins that form  
897 protein complexes than non-coexpressed cORF pairs, and this is consistent across different  
898 coexpression cutoffs. Coexpression was defined using the top 90th, 95th, 99th, and 99.9th  
899 percentile of all ORF pairs in the network (n = 62,204,406 ORF pairs). 90th percentile ( $p >$   
900 0.713) Odds ratio = 8.89; 95th percentile ( $p > 0.763$ ) Odds ratio = 9.59; 99th percentile ( $p >$   
901 0.836) Odds ratio = 9.23; 99.9th percentile ( $p > 0.906$ ) Odds ratio = 12.1; Fisher's exact test  $p <$   
902 2.2e-16 for all comparisons. Numbers above bars represent the number of ORF pairs in each  
903 category. Error bars represent the standard error of the proportion. A list of 408 protein  
904 complexes were retrieved from Pu et al. CYC2008 database [64]. Enrichments were calculated  
905 using only the 1,617 cORFs found in the CYC2008 database.

98

49

99

906 Supplementary Figure 5



907

908 Supplementary Figure 5 Coexpressed ORF pairs are more likely to have their promoters bound  
909 by a common TF than non-coexpressed ORF pairs, and this is true across different  
910 coexpression cutoffs and for canonical-canonical (cc), canonical-noncanonical (cn) and  
911 noncanonical-noncanonical (nn) ORF pairs. Coexpression was defined using the top 90th, 95th,  
912 99th, and 99.9th percentile of all ORF pairs in the network (n = 62,204,406 ORF pairs). 90th  
913 percentile ( $p > 0.713$ ): cc Odds ratio = 2.08, cn Odds ratio = 1.42, nn Odds ratio = 1.38; 95th  
914 percentile ( $p > 0.763$ ): cc Odds ratio = 2.38, cn Odds ratio = 1.50, nn Odds ratio = 1.45; 99th  
915 percentile ( $p > 0.836$ ): cc Odds ratio = 3.19, cn Odds ratio = 1.85, nn Odds ratio = 1.82; 99.9th  
916 percentile ( $p > 0.906$ ): cc Odds ratio = 4.57, cn Odds ratio = 3.10, nn Odds ratio = 4.29; \*\*\*\*:  
917 Fisher's exact test  $p < 2.2e-16$  for all comparisons. Error bars represent the standard error of

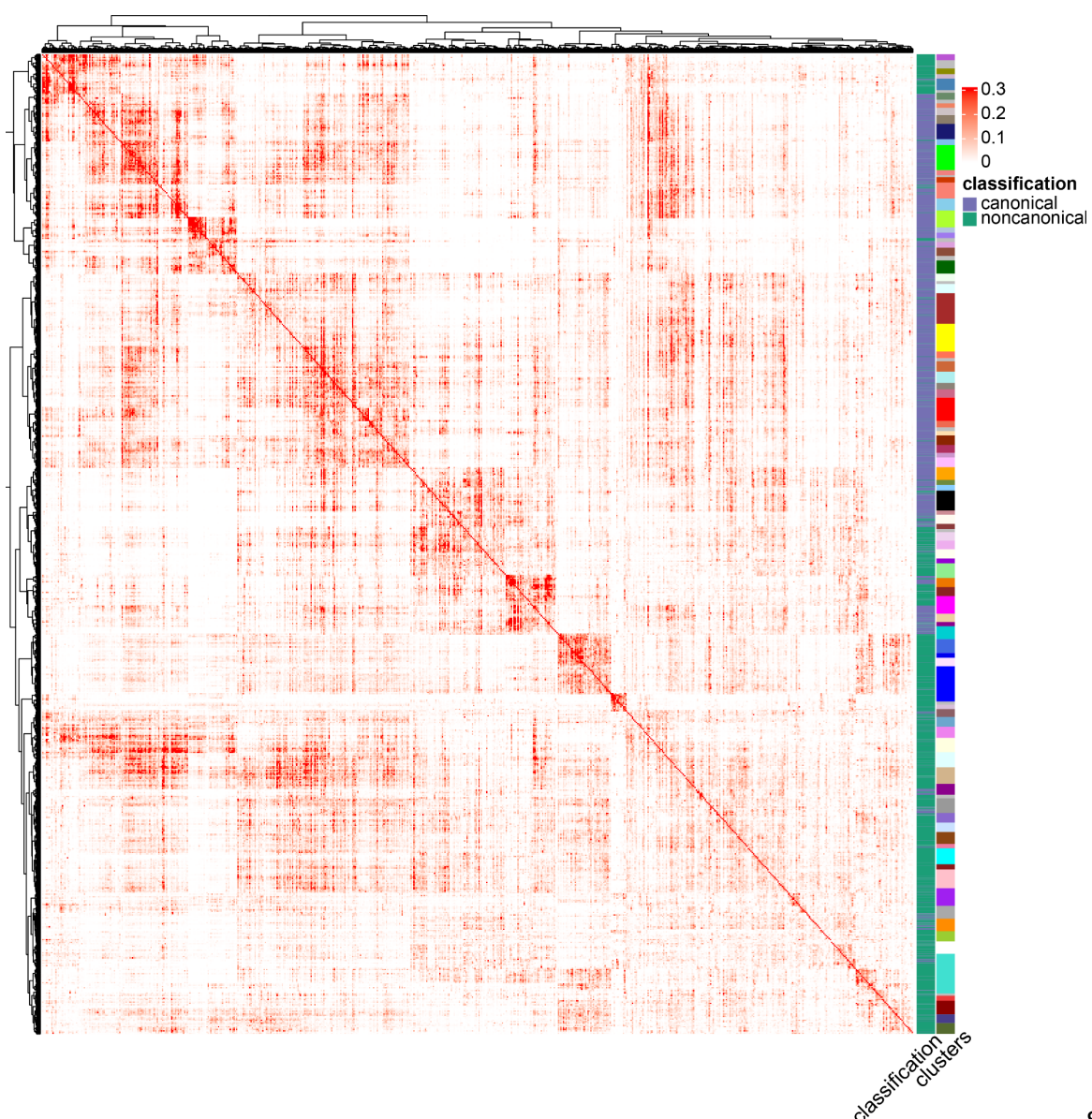
100

50

101

918 the proportion. Using a ChIP-exo dataset from Rossi et al. [65] containing DNA-binding  
919 information for 73 sequence-specific TFs, TF binding was defined as a ChIP-exo peak within  
920 200 bp upstream of the ORF's TSS. Only ORFs whose promoter was bound by at least one TF  
921 were considered. Numbers above bars represent the number of ORF pairs in each category.

922 **Supplementary Figure 6**



923

Supple

924 mentary Figure 6 Clustered matrix heatmap. Coexpression values are first transformed by

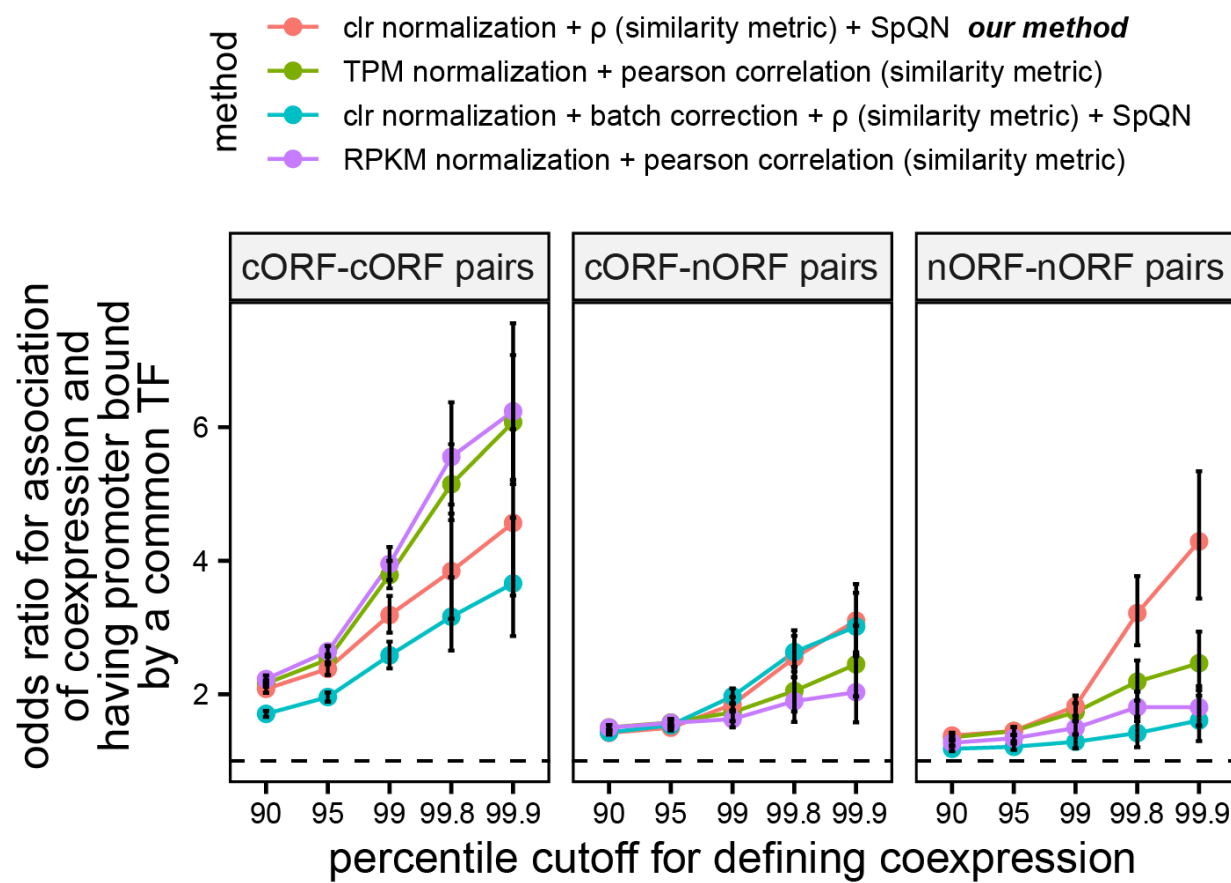
102

51

103

925 taking power of 12 and then WGCNA pipeline [70] is applied. Clusters are determined by cutting  
926 dendrograms (see methods for details). Colors on 'clusters' section represent the different  
927 clusters. Values of 0.3 and above are represented by red to show the structure of the heatmap.

928 **Supplementary Figure 7**



929

930 Supplementary Figure 7 Using clr normalization,  $\rho$  similarity metric and SpQN normalization  
931 leads to the highest odds ratios for nORF-nORF coexpressed pairs to also have their promoters  
932 bound by common TFs. Our method (*pink*) uses clr to transform the expression matrix, uses  
933 proportionality metric  $\rho$  to calculate coexpression and SpQN to normalize the coexpression  
934 matrix. Method TPM + pearson (*green*) uses TPM to normalize the expression matrix followed  
935 by Pearson correlation to calculate coexpression. Method clr + batch correction + rho + SpQN  
936 (*blue*) uses clr to transform the expression matrix, followed by removing the top principal

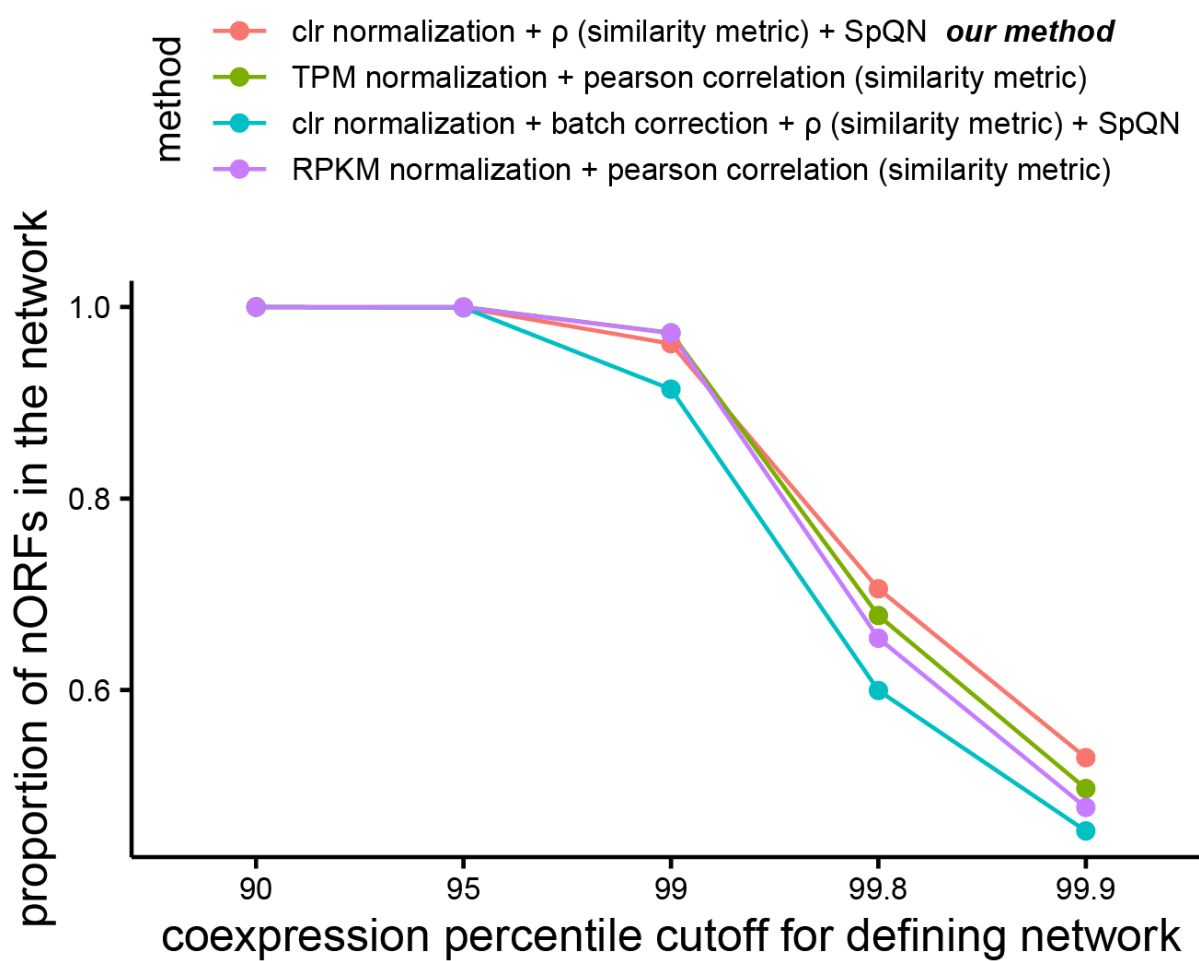
104

52

105

937 component of the clr expression matrix to do batch correction, followed by calculating  
938 coexpression using proportionality metric  $\rho$  and SpQN normalization of the coexpression matrix.  
939 Method RPKM + pearson correlation (purple) uses RPKM to normalize the expression matrix  
940 followed by Pearson correlation to calculate coexpression. Coexpression percentiles were  
941 determined using all ORF pairs ( $n = 62,204,406$  ORF pairs). All odds ratios are significant at  $p <$   
942  $2.15e-5$ , Fisher exact test. Batch correction performed by removing the top principal component  
943 on the clr transformed expression matrix. Error bars represent the 95% confidence interval of  
944 the odds ratio. Dashed line shows an odds ratio of 1.

945 **Supplementary Figure 8**



946

106

53

107

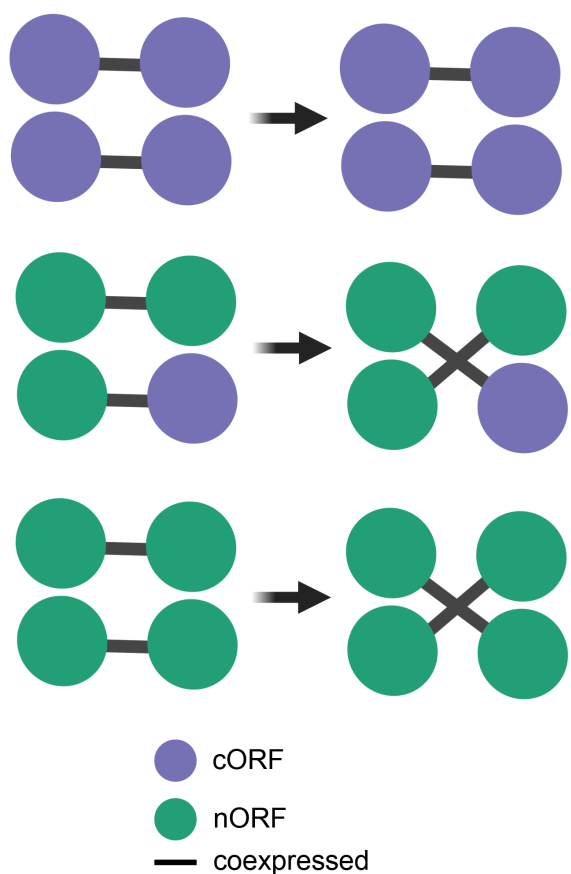
947 Supplementary Figure 8 Proportion of nORFs defined as coexpressed (and therefore included  
948 in the coexpression network) at various coexpression percentile cutoffs using four different  
949 methods. Our method (*pink*) uses clr to transform the expression matrix, uses proportionality  
950 metric  $\rho$  to calculate coexpression and SpQN to normalize the coexpression matrix. Method  
951 TPM + Pearson (*green*) uses TPM to normalize the expression matrix followed by Pearson  
952 correlation to calculate coexpression. Method  $\rho$  + batch correction (*blue*) uses clr to transform  
953 the expression matrix, followed by removing the top principal component of the clr expression  
954 matrix to do batch correction, followed by calculating coexpression using proportionality metric  $\rho$   
955 and SpQN normalization of the coexpression matrix. Method RPKM + pearson correlation  
956 (*purple*) uses RPKM to normalize the expression matrix followed by Pearson correlation to  
957 calculate coexpression. Coexpression percentiles were determined using all ORF pairs (n =  
958 62,204,406 ORF pairs).

108

54

109

959 Supplementary Figure 9



960

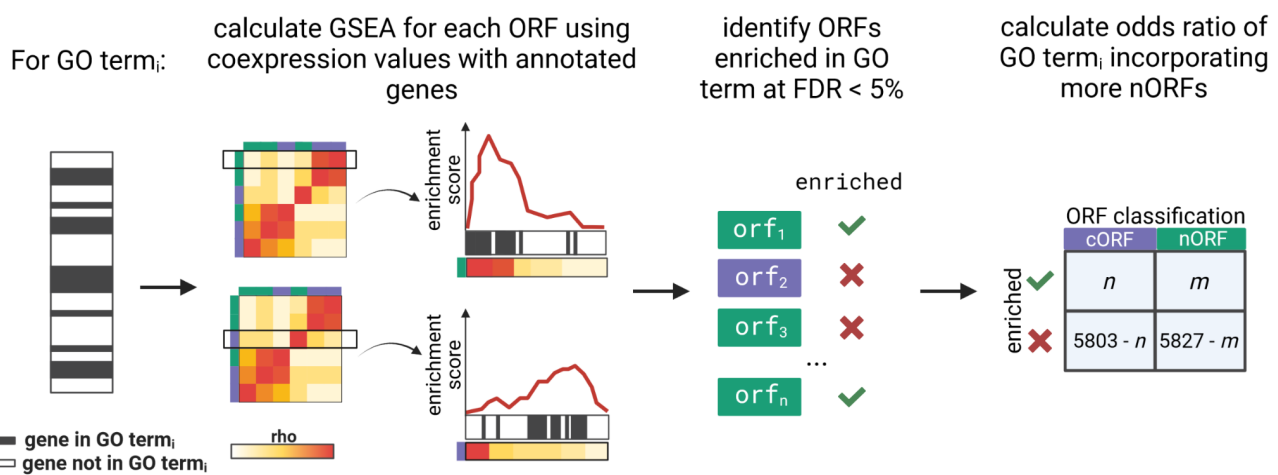
961 Supplementary Figure 9 Strategy for generating randomized networks. Edges between cORF-  
962 nORF and nORF-nORF pairs were swapped in a pairwise manner such that the degree of each  
963 node stayed the same. Edges between cORF-cORF pairs were not randomized.

110

55

111

## 964 Supplementary Figure 10



965

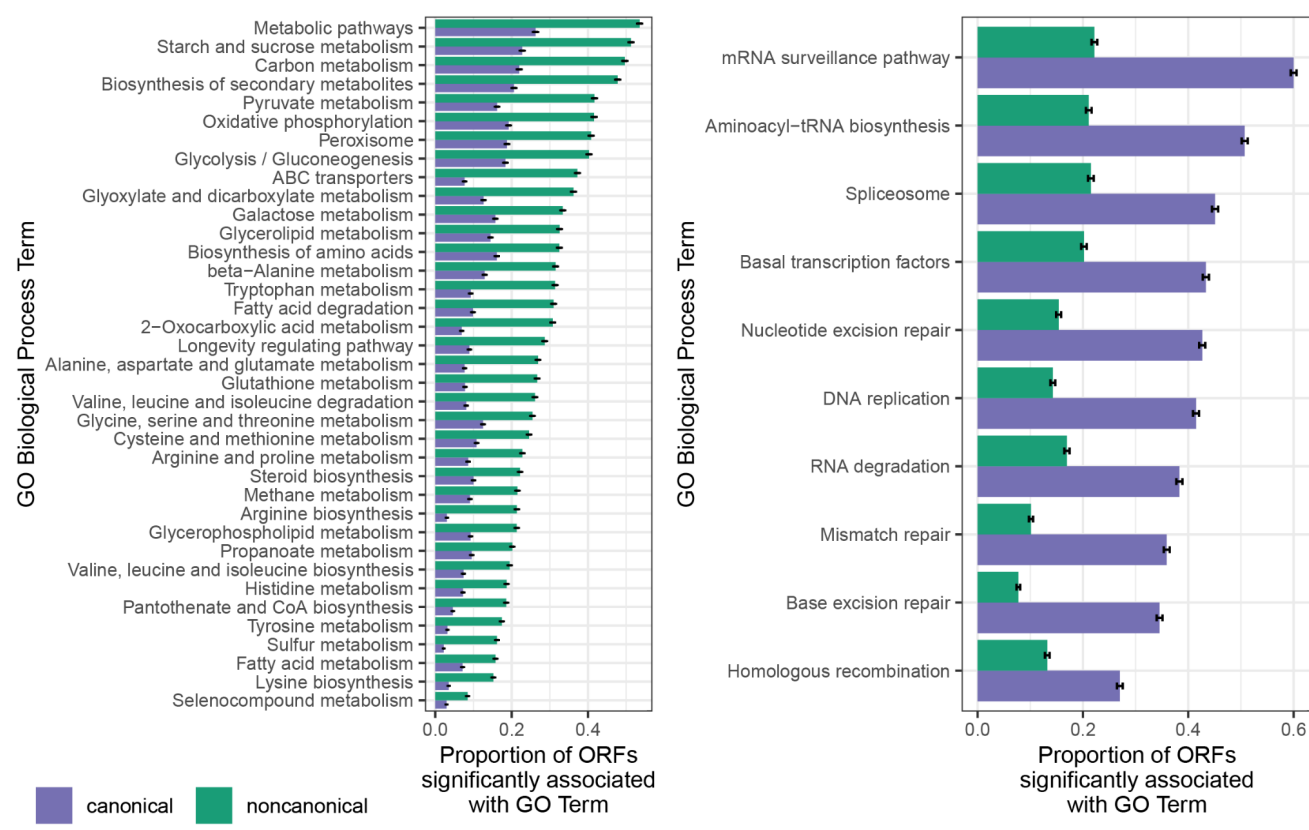
966 Supplementary Figure 10 GSEA pipeline using coexpression profiles to find GO terms that are  
967 more likely to incorporate nORFs.

112

56

113

968 Supplementary Figure 11

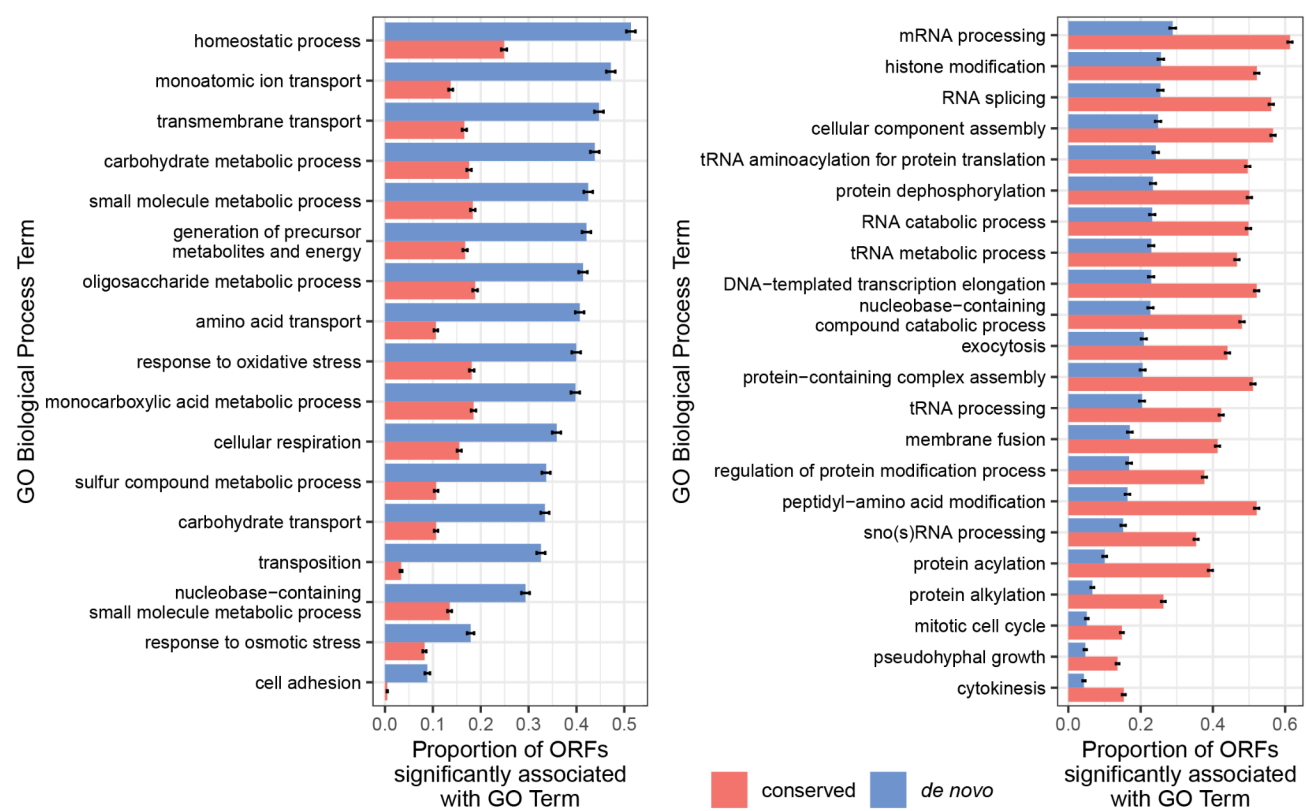


114

57

115

975 Supplementary Figure 12

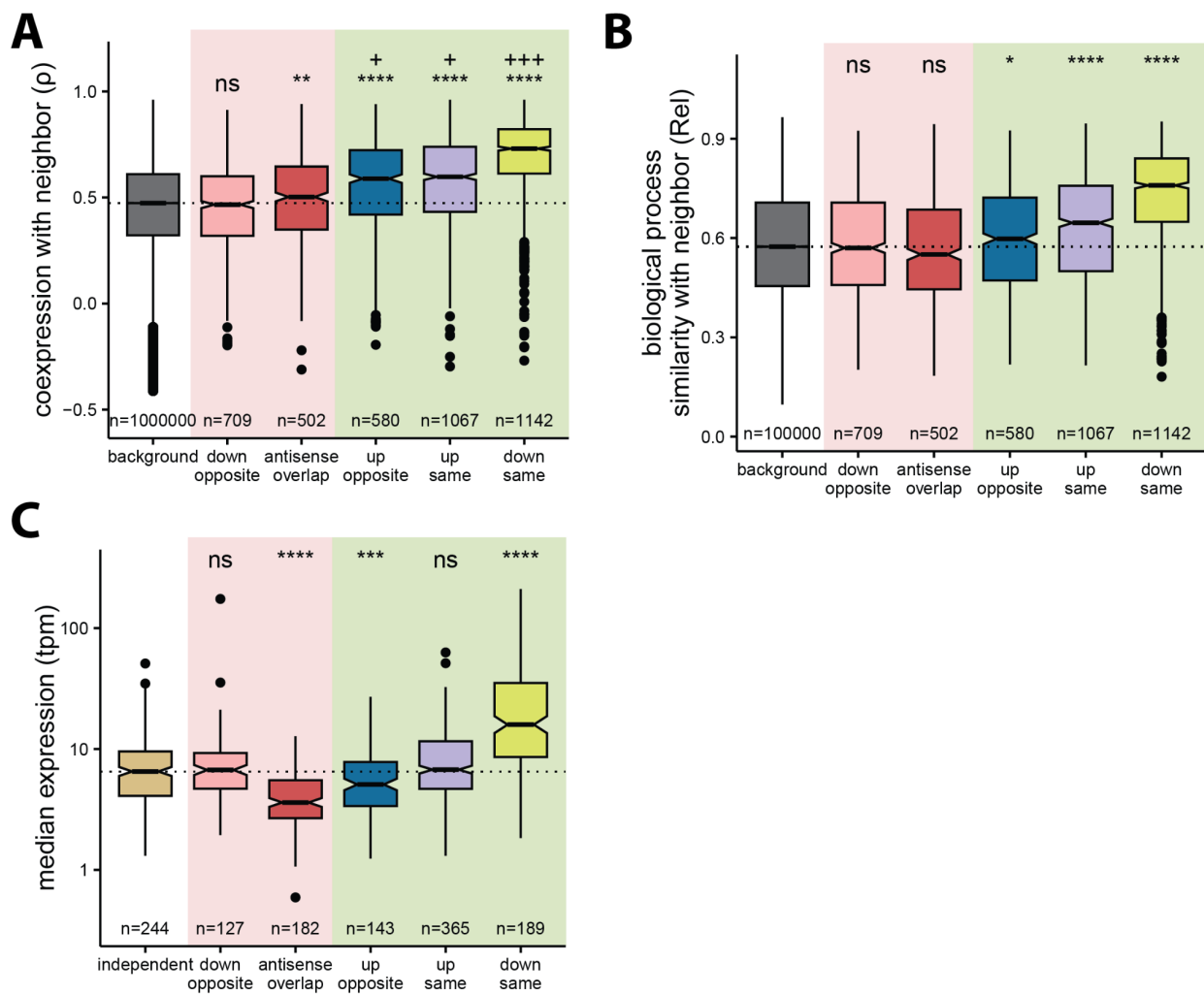


976

977 Supplementary Figure 12 GO terms that proportionally have more (*left*) (Odds ratio > 2, n = 35  
978 terms) or less (*right*) (Odds ratio < 0.5, n = 11 terms) GSEA enrichments with *de novo* ORFs  
979 compared to conserved ORFs (y-axis ordered by *de novo* ORF enrichment proportion from  
980 highest to lowest, BH adjusted FDR < 0.001 for all terms, Fisher's exact test). Error bars  
981 represent the standard error of the proportion.

117

## 982 Supplementary Figure 13



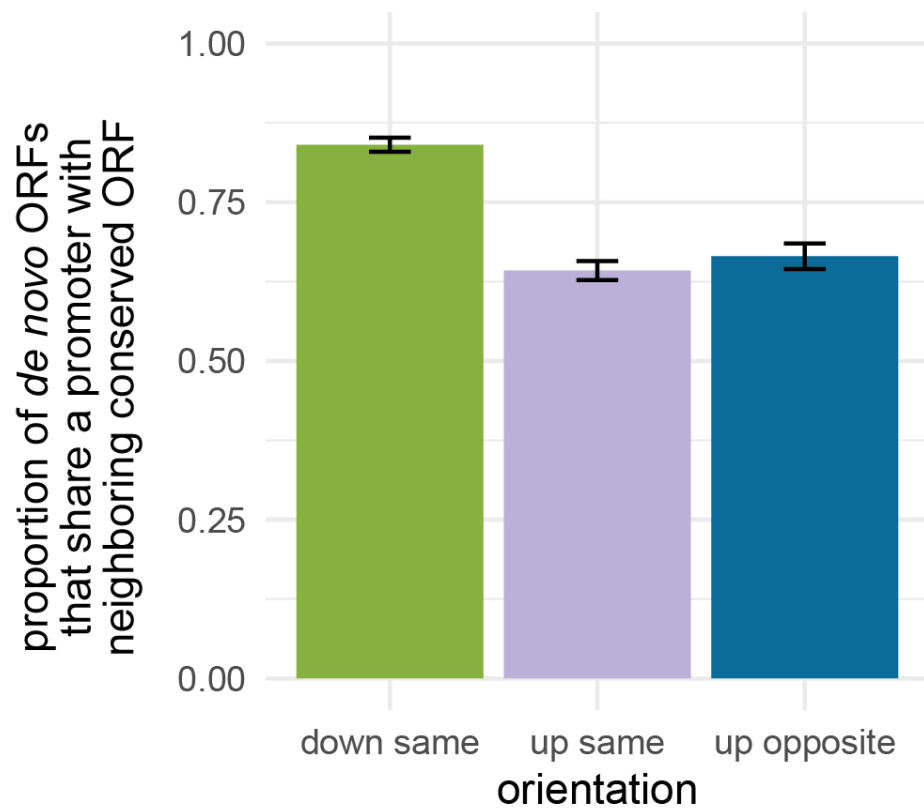
983

984 Supplementary Figure 13 A) Coexpression (y-axis) of *de novo* ORFs with neighboring  
985 conserved ORFs per orientation (x-axis). Down same *de novo* ORFs tend to be highly  
986 coexpressed with their neighbors; background: *de novo*-conserved ORF pairs located on  
987 different chromosomes. B) Biological process similarity (y-axis) of *de novo* ORFs with  
988 neighboring conserved ORFs per orientation (x-axis). Similarity measured by calculating  
989 semantic similarity between GSEA enrichments for neighboring *de novo*-conserved ORF pairs  
990 using relevance metric (0 = no similarity, 1 = perfect overlap); background: *de novo*-conserved  
991 ORF pairs located on different chromosomes. C) Median expression of *de novo* ORFs (y-axis)

119

992 per orientation (x-axis). *De novo* ORFs located downstream on the same strand as conserved  
993 ORFs have the highest expression among different orientations (considering only ORFs in only  
994 a single orientation, dashed box in panel 4D; independent: *de novo* ORFs located further than  
995 500 bp from all conserved ORFs). For panels A-B-C: Mann-Whitney U-test, \*\*\*\*:  $p \leq 0.0001$ , \*\*\*:  
996  $p \leq 0.001$ , \*\*:  $p \leq 0.01$ , \*:  $p \leq 0.05$ , ns: not-significant, +: small effect size (Cliff's  $d < 0.33$ ), ++:  
997 medium effect size (Cliff's  $d < 0.474$ ), +++: large effect size (Cliff's  $d \geq 0.474$ ); all orientations  
998 are compared to either background pairs (A, B) or to independent ORFs (C).

999 **Supplementary Figure 14**



1000

1001 Supplementary Figure 14 Proportion of *de novo* ORFs that share a promoter with their  
1002 neighboring conserved ORF. To determine if ORFs shared a promoter with neighbors we used  
1003 a publicly available TIF-seq dataset from Pelechano et al [65]. We defined down same or up  
1004 same ORFs as sharing a promoter if they mapped to the same transcript at least once, and

120

60

121

1005 defined up opposite ORFs as sharing a promoter if their respective transcripts did not have  
1006 overlapping TSSs. We found that 84% of down same ( $n = 174$ ), 64% of up same ( $n = 368$ ), and  
1007 66% of up opposite ( $n = 185$ ) *de novo* ORFs share a promoter with their neighboring conserved  
1008 ORF. Error bars represent the standard error of the proportion.

1009 

## References

1010 [1] Dujon B. The yeast genome project: what did we learn? *Trends Genet TIG* 1996;12:263–  
1011 70. [https://doi.org/10.1016/0168-9525\(96\)10027-5](https://doi.org/10.1016/0168-9525(96)10027-5).

1012 [2] Fisk DG, Ball CA, Dolinski K, Engel SR, Hong EL, Issel-Tarver L, et al. *Saccharomyces*  
1013 *cerevisiae* S288C genome annotation: a working hypothesis. *Yeast* Chichester Engl  
1014 2006;23:857–65. <https://doi.org/10.1002/yea.1400>.

1015 [3] Basrai MA, Hieter P, Boeke JD. Small Open Reading Frames: Beautiful Needles in the  
1016 Haystack. *Genome Res* 1997;7:768–71. <https://doi.org/10.1101/gr.7.8.768>.

1017 [4] Nagalakshmi U, Wang Z, Waern K, Shou C, Raha D, Gerstein M, et al. The  
1018 Transcriptional Landscape of the Yeast Genome Defined by RNA Sequencing. *Science*  
1019 2008;320:1344–9. <https://doi.org/10.1126/science.1158441>.

1020 [5] Ingolia NT, Ghaemmaghami S, Newman JRS, Weissman JS. Genome-Wide Analysis in  
1021 Vivo of Translation with Nucleotide Resolution Using Ribosome Profiling. *Science*  
1022 2009;324:218–23. <https://doi.org/10.1126/science.1168978>.

1023 [6] Ingolia NT, Brar GA, Stern-Ginossar N, Harris MS, Talhouarne GJS, Jackson SE, et al.  
1024 Ribosome Profiling Reveals Pervasive Translation Outside of Annotated Protein-Coding  
1025 Genes. *Cell Rep* 2014;8:1365–79. <https://doi.org/10.1016/j.celrep.2014.07.045>.

1026 [7] Bazzini AA, Johnstone TG, Christiano R, Mackowiak SD, Obermayer B, Fleming ES, et  
1027 al. Identification of small ORFs in vertebrates using ribosome footprinting and

123

1028 evolutionary conservation. *EMBO J* 2014;33:981–93.  
1029 <https://doi.org/10.1002/embj.201488411>.

1030 [8] Couso J-P, Patraquim P. Classification and function of small open reading frames. *Nat*  
1031 *Rev Mol Cell Biol* 2017;18:575–89. <https://doi.org/10.1038/nrm.2017.58>.

1032 [9] Lu S, Zhang J, Lian X, Sun L, Meng K, Chen Y, et al. A hidden human proteome encoded  
1033 by ‘non-coding’ genes. *Nucleic Acids Res* 2019;47:8111–25.  
1034 <https://doi.org/10.1093/nar/gkz646>.

1035 [10] Chen J, Brunner A-D, Cogan JZ, Nuñez JK, Fields AP, Adamson B, et al. Pervasive  
1036 functional translation of noncanonical human open reading frames. *Science*  
1037 2020;367:1140–6. <https://doi.org/10.1126/science.aay0262>.

1038 [11] Orr MW, Mao Y, Storz G, Qian S-B. Alternative ORFs and small ORFs: shedding light on  
1039 the dark proteome. *Nucleic Acids Res* 2020;48:1029–42.  
1040 <https://doi.org/10.1093/nar/gkz734>.

1041 [12] Vitorino R, Guedes S, Amado F, Santos M, Akimitsu N. The role of micropeptides in  
1042 biology. *Cell Mol Life Sci* 2021;78:3285–98. <https://doi.org/10.1007/s00018-020-03740-3>.

1043 [13] Prensner JR, Enache OM, Luria V, Krug K, Clauser KR, Dempster JM, et al.  
1044 Noncanonical open reading frames encode functional proteins essential for cancer cell  
1045 survival. *Nat Biotechnol* 2021;39:697–704. <https://doi.org/10.1038/s41587-020-00806-2>.

1046 [14] Wacholder A, Parikh SB, Coelho NC, Acar O, Houghton C, Chou L, et al. A vast  
1047 evolutionarily transient translatome contributes to phenotype and fitness. *Cell Syst*  
1048 2023;14:363-381.e8. <https://doi.org/10.1016/j.cels.2023.04.002>.

1049 [15] Vakirlis N, Acar O, Hsu B, Castilho Coelho N, Van Oss SB, Wacholder A, et al. De novo  
1050 emergence of adaptive membrane proteins from thymine-rich genomic sequences. *Nat*  
1051 *Commun* 2020;11:781. <https://doi.org/10.1038/s41467-020-14500-z>.

124

62

125

1052 [16] Arnoult N, Correia A, Ma J, Merlo A, Garcia-Gomez S, Maric M, et al. Regulation of DNA  
1053 repair pathway choice in S and G2 phases by the NHEJ inhibitor CYREN. *Nature*  
1054 2017;549:548–52. <https://doi.org/10.1038/nature24023>.

1055 [17] Anderson DM, Anderson KM, Chang C-L, Makarewich CA, Nelson BR, McAnally JR, et  
1056 al. A Micropeptide Encoded by a Putative Long Noncoding RNA Regulates Muscle  
1057 Performance. *Cell* 2015;160:595–606. <https://doi.org/10.1016/j.cell.2015.01.009>.

1058 [18] Magny EG, Pueyo JI, Pearl FMG, Cespedes MA, Niven JE, Bishop SA, et al. Conserved  
1059 Regulation of Cardiac Calcium Uptake by Peptides Encoded in Small Open Reading  
1060 Frames. *Science* 2013;341:1116–20. <https://doi.org/10.1126/science.1238802>.

1061 [19] Matsumoto A, Pasut A, Matsumoto M, Yamashita R, Fung J, Monteleone E, et al.  
1062 mTORC1 and muscle regeneration are regulated by the LINC00961-encoded SPAR  
1063 polypeptide. *Nature* 2017;541:228–32. <https://doi.org/10.1038/nature21034>.

1064 [20] Jackson R, Kroehling L, Khitun A, Bailis W, Jarret A, York AG, et al. The translation of  
1065 non-canonical open reading frames controls mucosal immunity. *Nature* 2018;564:434–8.  
1066 <https://doi.org/10.1038/s41586-018-0794-7>.

1067 [21] Bhatta A, Atianand M, Jiang Z, Crabtree J, Blin J, Fitzgerald KA. A Mitochondrial  
1068 Micropeptide Is Required for Activation of the Nlrp3 Inflammasome. *J Immunol*  
1069 2020;204:428–37. <https://doi.org/10.4049/jimmunol.1900791>.

1070 [22] Niu X, Zhang J, Zhang L, Hou Y, Pu S, Chu A, et al. Weighted Gene Co-Expression  
1071 Network Analysis Identifies Critical Genes in the Development of Heart Failure After  
1072 Acute Myocardial Infarction. *Front Genet* 2019;10.  
1073 <https://doi.org/10.3389/fgene.2019.01214>.

1074 [23] Wright BW, Yi Z, Weissman JS, Chen J. The dark proteome: translation from  
1075 noncanonical open reading frames. *Trends Cell Biol* 2021.  
1076 <https://doi.org/10.1016/j.tcb.2021.10.010>.

126

63

127

1077 [24] Carvunis A-R, Rolland T, Wapinski I, Calderwood MA, Yildirim MA, Simonis N, et al.  
1078 Proto-genes and *de novo* gene birth. *Nature* 2012;487:370–4.  
1079 <https://doi.org/10.1038/nature11184>.

1080 [25] Van Oss SB, Carvunis A-R. *De novo* gene birth. *PLOS Genet* 2019;15:e1008160.  
1081 <https://doi.org/10.1371/journal.pgen.1008160>.

1082 [26] Sandmann C-L, Schulz JF, Ruiz-Orera J, Kirchner M, Ziehm M, Adami E, et al.  
1083 Evolutionary origins and interactomes of human, young microproteins and small peptides  
1084 translated from short open reading frames. *Mol Cell* 2023;83:994-1011.e18.  
1085 <https://doi.org/10.1016/j.molcel.2023.01.023>.

1086 [27] Zhang W, Landback P, Gschwend AR, Shen B, Long M. New genes drive the evolution of  
1087 gene interaction networks in the human and mouse genomes. *Genome Biol* 2015;16:202.  
1088 <https://doi.org/10.1186/s13059-015-0772-4>.

1089 [28] Abrusán G. Integration of New Genes into Cellular Networks, and Their Structural  
1090 Maturation. *Genetics* 2013;195:1407–17. <https://doi.org/10.1534/genetics.113.152256>.

1091 [29] Capra JA, Pollard KS, Singh M. Novel genes exhibit distinct patterns of function  
1092 acquisition and network integration. *Genome Biol* 2010;11:R127.  
1093 <https://doi.org/10.1186/gb-2010-11-12-r127>.

1094 [30] Housman G, Ulitsky I. Methods for distinguishing between protein-coding and long  
1095 noncoding RNAs and the elusive biological purpose of translation of long noncoding  
1096 RNAs. *Biochim Biophys Acta - Gene Regul Mech* 2016;1859:31–40.  
1097 <https://doi.org/10.1016/j.bbagr.2015.07.017>.

1098 [31] Pertea M, Shumate A, Pertea G, Varabyou A, Breitwieser FP, Chang Y-C, et al. CHESS:  
1099 a new human gene catalog curated from thousands of large-scale RNA sequencing  
1100 experiments reveals extensive transcriptional noise. *Genome Biol* 2018;19:208.  
1101 <https://doi.org/10.1186/s13059-018-1590-2>.

128

64

129

1102 [32] Xu H, Li C, Xu C, Zhang J. Chance promoter activities illuminate the origins of eukaryotic  
1103 intergenic transcriptions. *Nat Commun* 2023;14:1826. <https://doi.org/10.1038/s41467-023-37610-w>.

1104

1105 [33] Schlötterer C. Genes from scratch – the evolutionary fate of de novo genes. *Trends Genet* 2015;31:215–9. <https://doi.org/10.1016/j.tig.2015.02.007>.

1106

1107 [34] Zhao L, Saelao P, Jones CD, Begun DJ. Origin and spread of de novo genes in  
1108 *Drosophila melanogaster* populations. *Science* 2014;343:769–72.  
<https://doi.org/10.1126/science.1248286>.

1109

1110 [35] Zhuang X, Yang C, Murphy KR, Cheng C-HC. Molecular mechanism and history of non-  
1111 sense to sense evolution of antifreeze glycoprotein gene in northern gadids. *Proc Natl Acad Sci* 2019;116:4400–5. <https://doi.org/10.1073/pnas.1817138116>.

1112

1113 [36] Ruiz-Orera J, Hernandez-Rodriguez J, Chiva C, Sabidó E, Kondova I, Bontrop R, et al.  
1114 Origins of De Novo Genes in Human and Chimpanzee. *PLOS Genet* 2015;11:e1005721.  
<https://doi.org/10.1371/journal.pgen.1005721>.

1115

1116 [37] Vakirlis N, Vance Z, Duggan KM, McLysaght A. De novo birth of functional microproteins  
1117 in the human lineage. *Cell Rep* 2022;41:111808.  
<https://doi.org/10.1016/j.celrep.2022.111808>.

1118

1119 [38] Majic P, Payne JL. Enhancers Facilitate the Birth of De Novo Genes and Gene  
1120 Integration into Regulatory Networks. *Mol Biol Evol* 2020;37:1165–78.  
<https://doi.org/10.1093/molbev/msz300>.

1121

1122 [39] Ruiz-Orera J, Villanueva-Cañas JL, Albà MM. Evolution of new proteins from translated  
1123 sORFs in long non-coding RNAs. *Exp Cell Res* 2020;391:111940.  
<https://doi.org/10.1016/j.yexcr.2020.111940>.

1124

1125 [40] Chen J-Y, Shen QS, Zhou W-Z, Peng J, He BZ, Li Y, et al. Emergence, Retention and  
1126 Selection: A Trilogy of Origination for Functional De Novo Proteins from Ancestral

130

65

131

1127 LncRNAs in Primates. PLOS Genet 2015;11:e1005391.  
1128 <https://doi.org/10.1371/journal.pgen.1005391>.

1129 [41] Vakirlis N, Hebert AS, Opulente DA, Achaz G, Hittinger CT, Fischer G, et al. A Molecular  
1130 Portrait of De Novo Genes in Yeasts. Mol Biol Evol 2018;35:631–45.  
1131 <https://doi.org/10.1093/molbev/msx315>.

1132 [42] Neme R, Tautz D. Fast turnover of genome transcription across evolutionary time  
1133 exposes entire non-coding DNA to de novo gene emergence. eLife 2016;5:e09977.  
1134 <https://doi.org/10.7554/eLife.09977>.

1135 [43] Knowles DG, McLysaght A. Recent de novo origin of human protein-coding genes.  
1136 Genome Res 2009;19:1752–9. <https://doi.org/10.1101/gr.095026.109>.

1137 [44] Ebisuya M, Yamamoto T, Nakajima M, Nishida E. Ripples from neighbouring  
1138 transcription. Nat Cell Biol 2008;10:1106–13. <https://doi.org/10.1038/ncb1771>.

1139 [45] Ghanbarian AT, Hurst LD. Neighboring Genes Show Correlated Evolution in Gene  
1140 Expression. Mol Biol Evol 2015;32:1748–66. <https://doi.org/10.1093/molbev/msv053>.

1141 [46] Ji Z, Song R, Regev A, Struhl K. Many lncRNAs, 5'UTRs, and pseudogenes are  
1142 translated and some are likely to express functional proteins. eLife 2015;4:e08890.  
1143 <https://doi.org/10.7554/eLife.08890>.

1144 [47] Li J, Singh U, Arendsee Z, Wurtele ES. Landscape of the Dark Transcriptome Revealed  
1145 Through Re-mining Massive RNA-Seq Data. Front Genet 2021;12.

1146 [48] O'Meara TR, O'Meara MJ. DeORFanizing *Candida albicans* Genes using Coexpression.  
1147 MSphere 2021;6:e01245-20. <https://doi.org/10.1128/mSphere.01245-20>.

1148 [49] Chothani SP, Adami E, Widjaja AA, Langley SR, Viswanathan S, Pua CJ, et al. A high-  
1149 resolution map of human RNA translation. Mol Cell 2022;82:2885-2899.e8.  
1150 <https://doi.org/10.1016/j.molcel.2022.06.023>.

132

66

133

1151 [50] Kim SK, Lund J, Kiraly M, Duke K, Jiang M, Stuart JM, et al. A Gene Expression Map for  
1152 *Caenorhabditis elegans*. *Science* 2001;293:2087–92.  
1153 <https://doi.org/10.1126/science.1061603>.

1154 [51] Stuart JM, Segal E, Koller D, Kim SK. A Gene-Coexpression Network for Global  
1155 Discovery of Conserved Genetic Modules. *Science* 2003;302:249–55.  
1156 <https://doi.org/10.1126/science.1087447>.

1157 [52] Yang Y, Han L, Yuan Y, Li J, Hei N, Liang H. Gene co-expression network analysis  
1158 reveals common system-level properties of prognostic genes across cancer types. *Nat*  
1159 *Commun* 2014;5:3231. <https://doi.org/10.1038/ncomms4231>.

1160 [53] Voineagu I, Wang X, Johnston P, Lowe JK, Tian Y, Horvath S, et al. Transcriptomic  
1161 analysis of autistic brain reveals convergent molecular pathology. *Nature* 2011;474:380–  
1162 4. <https://doi.org/10.1038/nature10110>.

1163 [54] Xue Z, Huang K, Cai C, Cai L, Jiang C, Feng Y, et al. Genetic programs in human and  
1164 mouse early embryos revealed by single-cell RNA sequencing. *Nature* 2013;500:593–7.  
1165 <https://doi.org/10.1038/nature12364>.

1166 [55] Lee J, Shah M, Ballouz S, Crow M, Gillis J. CoCoCoNet: conserved and comparative co-  
1167 expression across a diverse set of species. *Nucleic Acids Res* 2020;48:W566–71.  
1168 <https://doi.org/10.1093/nar/gkaa348>.

1169 [56] van Dam S, Võsa U, van der Graaf A, Franke L, de Magalhães JP. Gene co-expression  
1170 analysis for functional classification and gene–disease predictions. *Brief Bioinform*  
1171 2018;19:575–92. <https://doi.org/10.1093/bib/bbw139>.

1172 [57] Yin W, Mendoza L, Monzon-Sandoval J, Urrutia AO, Gutierrez H. Emergence of co-  
1173 expression in gene regulatory networks. *PLOS ONE* 2021;16:e0247671.  
1174 <https://doi.org/10.1371/journal.pone.0247671>.

1175 [58] Hanada K, Higuchi-Takeuchi M, Okamoto M, Yoshizumi T, Shimizu M, Nakaminami K, et  
1176 al. Small open reading frames associated with morphogenesis are hidden in plant

135

1177 genomes. *Proc Natl Acad Sci* 2013;110:2395–400.

1178 <https://doi.org/10.1073/pnas.1213958110>.

1179 [59] Bashir K, Hanada K, Shimizu M, Seki M, Nakanishi H, Nishizawa NK. Transcriptomic

1180 analysis of rice in response to iron deficiency and excess. *Rice* 2014;7:18.

1181 <https://doi.org/10.1186/s12284-014-0018-1>.

1182 [60] Stiens J, Tan YY, Joyce R, Arnvig KB, Kendall SL, Nobeli I. Using a Whole Genome Co-

1183 expression Network to Inform the Functional Characterisation of Predicted Genomic

1184 Elements from *Mycobacterium tuberculosis* Transcriptomic Data

1185 2022:2022.06.22.497203. <https://doi.org/10.1101/2022.06.22.497203>.

1186 [61] Li H, Xiao L, Zhang L, Wu J, Wei B, Sun N, et al. FSPP: A Tool for Genome-Wide

1187 Prediction of smORF-Encoded Peptides and Their Functions. *Front Genet* 2018;9.

1188 <https://doi.org/10.3389/fgene.2018.00096>.

1189 [62] Wang Y, Hicks SC, Hansen KD. Addressing the mean-correlation relationship in co-

1190 expression analysis. *PLOS Comput Biol* 2022;18:e1009954.

1191 <https://doi.org/10.1371/journal.pcbi.1009954>.

1192 [63] Crow M, Paul A, Ballouz S, Huang ZJ, Gillis J. Exploiting single-cell expression to

1193 characterize co-expression replicability. *Genome Biol* 2016;17:101.

1194 <https://doi.org/10.1186/s13059-016-0964-6>.

1195 [64] Pu S, Wong J, Turner B, Cho E, Wodak SJ. Up-to-date catalogues of yeast protein

1196 complexes. *Nucleic Acids Res* 2009;37:825–31. <https://doi.org/10.1093/nar/gkn1005>.

1197 [65] Rossi MJ, Kuntala PK, Lai WKM, Yamada N, Bajjatia N, Mittal C, et al. A high-resolution

1198 protein architecture of the budding yeast genome. *Nature* 2021;592:309–14.

1199 <https://doi.org/10.1038/s41586-021-03314-8>.

1200 [66] Pelechano V, Wei W, Steinmetz LM. Extensive transcriptional heterogeneity revealed by

1201 isoform profiling. *Nature* 2013;497:127–31. <https://doi.org/10.1038/nature12121>.

137

1202 [67] Cherry JM, Hong EL, Amundsen C, Balakrishnan R, Binkley G, Chan ET, et al.  
1203 Saccharomyces Genome Database: the genomics resource of budding yeast. Nucleic  
1204 Acids Res 2012;40:D700–5. <https://doi.org/10.1093/nar/gkr1029>.

1205 [68] Skinnider MA, Squair JW, Foster LJ. Evaluating measures of association for single-cell  
1206 transcriptomics. Nat Methods 2019;16:381–6. <https://doi.org/10.1038/s41592-019-0372-4>.

1207 [69] Quinn TP, Richardson MF, Lovell D, Crowley TM. propr: An R-package for Identifying  
1208 Proportionally Abundant Features Using Compositional Data Analysis. Sci Rep  
1209 2017;7:16252. <https://doi.org/10.1038/s41598-017-16520-0>.

1210 [70] Langfelder P, Horvath S. WGCNA: an R package for weighted correlation network  
1211 analysis. BMC Bioinformatics 2008;9:559. <https://doi.org/10.1186/1471-2105-9-559>.

1212 [71] Ballouz S, Verleyen W, Gillis J. Guidance for RNA-seq co-expression network  
1213 construction and analysis: safety in numbers. Bioinformatics 2015;31:2123–30.  
1214 <https://doi.org/10.1093/bioinformatics/btv118>.

1215 [72] Parsana P, Ruberman C, Jaffe AE, Schatz MC, Battle A, Leek JT. Addressing  
1216 confounding artifacts in reconstruction of gene co-expression networks. Genome Biol  
1217 2019;20:94. <https://doi.org/10.1186/s13059-019-1700-9>.

1218 [73] Chang W, Cheng J, Allaire J, Sievert C, Schloerke B, Xie Y, et al. shiny: Web application  
1219 framework for R. 2023.

1220 [74] Fruchterman TMJ, Reingold EM. Graph drawing by force-directed placement. Softw Pract  
1221 Exp 1991;21:1129–64. <https://doi.org/10.1002/spe.4380211102>.

1222 [75] Krogh A, Larsson B, von Heijne G, Sonnhammer ELL. Predicting transmembrane protein  
1223 topology with a hidden markov model: application to complete genomes. J Mol Biol  
1224 2001;305:567–80. <https://doi.org/10.1006/jmbi.2000.4315>.

1225 [76] Ciccarelli M, Masser AE, Kaimal JM, Planells J, Andréasson C. Genetic inactivation of  
1226 essential HSF1 reveals an isolated transcriptional stress response selectively induced by  
1227 protein misfolding 2023:2023.05.05.539545. <https://doi.org/10.1101/2023.05.05.539545>.

138

69

139

1228 [77] Subramanian A, Tamayo P, Mootha VK, Mukherjee S, Ebert BL, Gillette MA, et al. Gene  
1229 set enrichment analysis: A knowledge-based approach for interpreting genome-wide  
1230 expression profiles. *Proc Natl Acad Sci* 2005;102:15545–50.  
1231 <https://doi.org/10.1073/pnas.0506580102>.

1232 [78] Kanehisa M, Sato Y, Kawashima M, Furumichi M, Tanabe M. KEGG as a reference  
1233 resource for gene and protein annotation. *Nucleic Acids Res* 2016;44:D457–62.  
1234 <https://doi.org/10.1093/nar/gkv1070>.

1235 [79] Hu Z, Killion PJ, Iyer VR. Genetic reconstruction of a functional transcriptional regulatory  
1236 network. *Nat Genet* 2007;39:683–7. <https://doi.org/10.1038/ng2012>.

1237 [80] Marion RM, Regev A, Segal E, Barash Y, Koller D, Friedman N, et al. Sfp1 is a stress-  
1238 and nutrient-sensitive regulator of ribosomal protein gene expression. *Proc Natl Acad Sci*  
1239 2004;101:14315–22. <https://doi.org/10.1073/pnas.0405353101>.

1240 [81] Masser AE, Kang W, Roy J, Mohanakrishnan Kaimal J, Quintana-Cordero J, Friedländer  
1241 MR, et al. Cytoplasmic protein misfolding titrates Hsp70 to activate nuclear Hsf1. *eLife*  
1242 2019;8:e47791. <https://doi.org/10.7554/eLife.47791>.

1243 [82] Schlicker A, Domingues FS, Rahnenführer J, Lengauer T. A new measure for functional  
1244 similarity of gene products based on Gene Ontology. *BMC Bioinformatics* 2006;7:302.  
1245 <https://doi.org/10.1186/1471-2105-7-302>.

1246 [83] Wei W, Pelechano V, Järvelin AI, Steinmetz LM. Functional consequences of bidirectional  
1247 promoters. *Trends Genet* 2011;27:267–76. <https://doi.org/10.1016/j.tig.2011.04.002>.

1248 [84] Zrimec J, Börlin CS, Buric F, Muhammad AS, Chen R, Siewers V, et al. Deep learning  
1249 suggests that gene expression is encoded in all parts of a co-evolving interacting gene  
1250 regulatory structure. *Nat Commun* 2020;11:6141. [https://doi.org/10.1038/s41467-020-19921-4](https://doi.org/10.1038/s41467-020-<br/>1251 19921-4).

141

1252 [85] Blevins WR, Ruiz-Orera J, Messeguer X, Blasco-Moreno B, Villanueva-Cañas JL,  
1253 Espinar L, et al. Uncovering de novo gene birth in yeast using deep transcriptomics. *Nat  
1254 Commun* 2021;12:604. <https://doi.org/10.1038/s41467-021-20911-3>.

1255 [86] Khitun A, Ness TJ, Slavoff SA. Small open reading frames and cellular stress responses.  
1256 *Mol Omics* 2019;15:108–16. <https://doi.org/10.1039/C8MO00283E>.

1257 [87] Wilson BA, Masel J. Putatively Noncoding Transcripts Show Extensive Association with  
1258 Ribosomes. *Genome Biol Evol* 2011;3:1245–52. <https://doi.org/10.1093/gbe/evr099>.

1259 [88] Li D, Yan Z, Lu L, Jiang H, Wang W. Pleiotropy of the de novo-originated gene MDF1. *Sci  
1260 Rep* 2014;4. <https://doi.org/10.1038/srep07280>.

1261 [89] Frumkin I, Laub MT. Selection of a de novo gene that can promote survival of *E. coli* by  
1262 modulating protein homeostasis pathways 2023:2023.02.07.527531.  
1263 <https://doi.org/10.1101/2023.02.07.527531>.

1264 [90] Li D, Dong Y, Jiang Y, Jiang H, Cai J, Wang W. A de novo originated gene depresses  
1265 budding yeast mating pathway and is repressed by the protein encoded by its antisense  
1266 strand. *Cell Res* 2010;20:408–20. <https://doi.org/10.1038/cr.2010.31>.

1267 [91] Pagé N, Gérard-Vincent M, Ménard P, Beaulieu M, Azuma M, Dijkgraaf GJP, et al. A  
1268 *Saccharomyces cerevisiae* Genome-Wide Mutant Screen for Altered Sensitivity to K1  
1269 Killer Toxin. *Genetics* 2003;163:875–94. <https://doi.org/10.1093/genetics/163.3.875>.

1270 [92] Tassios E, Nikolaou C, Vakirlis N. Intergenic Regions of *Saccharomycotina* Yeasts are  
1271 Enriched in Potential to Encode Transmembrane Domains. *Mol Biol Evol*  
1272 2023;40:msad059. <https://doi.org/10.1093/molbev/msad059>.

1273 [93] Peng J, Zhao L. The origin and structural evolution of de novo genes in *Drosophila*  
1274 2023:2023.03.13.532420. <https://doi.org/10.1101/2023.03.13.532420>.

1275 [94] Kesner JS, Chen Z, Aparicio AA, Wu X. A unified model for the surveillance of translation  
1276 in diverse noncoding sequences 2022:2022.07.20.500724.  
1277 <https://doi.org/10.1101/2022.07.20.500724>.

143

1278 [95] Slavoff SA, Mitchell AJ, Schwaid AG, Cabili MN, Ma J, Levin JZ, et al. Peptidomic  
1279 discovery of short open reading frame–encoded peptides in human cells. *Nat Chem Biol*  
1280 2013;9:59–64. <https://doi.org/10.1038/nchembio.1120>.

1281 [96] Zhang S, Reljić B, Liang C, Kerouanton B, Francisco JC, Peh JH, et al. Mitochondrial  
1282 peptide BRAWNIN is essential for vertebrate respiratory complex III assembly. *Nat*  
1283 *Commun* 2020;11:1312. <https://doi.org/10.1038/s41467-020-14999-2>.

1284 [97] Leong AZ-X, Lee PY, Mohtar MA, Syafruddin SE, Pung Y-F, Low TY. Short open reading  
1285 frames (sORFs) and microproteins: an update on their identification and validation  
1286 measures. *J Biomed Sci* 2022;29:19. <https://doi.org/10.1186/s12929-022-00802-5>.

1287 [98] Mayr C. What Are 3' UTRs Doing? *Cold Spring Harb Perspect Biol* 2019;11:a034728.  
1288 <https://doi.org/10.1101/cshperspect.a034728>.

1289 [99] Vilborg A, Passarelli MC, Yario TA, Tycowski KT, Steitz JA. Widespread Inducible  
1290 Transcription Downstream of Human Genes. *Mol Cell* 2015;59:449–61.  
1291 <https://doi.org/10.1016/j.molcel.2015.06.016>.

1292 [100] Wu Q, Wright M, Gogol MM, Bradford WD, Zhang N, Bazzini AA. Translation of small  
1293 downstream ORFs enhances translation of canonical main open reading frames. *EMBO J*  
1294 2020;39:e104763. <https://doi.org/10.15252/embj.2020104763>.

1295 [101] Wu B, Cox MP. Characterization of Bicistronic Transcription in Budding Yeast. *MSystems*  
1296 2021;6:e01002-20. <https://doi.org/10.1128/mSystems.01002-20>.

1297 [102] Kustatscher G, Grabowski P, Rappsilber J. Pervasive coexpression of spatially proximal  
1298 genes is buffered at the protein level. *Mol Syst Biol* 2017;13:937.  
1299 <https://doi.org/10.15252/msb.20177548>.

1300 [103] *Saccharomyces Genome Database | SGD* n.d. <https://www.yeastgenome.org/> (accessed  
1301 January 20, 2021).

1302 [104] Quinlan AR, Hall IM. BEDTools: a flexible suite of utilities for comparing genomic  
1303 features. *Bioinformatics* 2010;26:841–2. <https://doi.org/10.1093/bioinformatics/btq033>.

144

72

145

1304 [105] Krueger F, James F, Ewels P, Afyounian E, Weinstein M, Schuster-Boeckler B, et al.  
1305 FelixKrueger/TrimGalore 2023. <https://doi.org/10.5281/zenodo.7598955>.

1306 [106] Patro R, Duggal G, Love MI, Irizarry RA, Kingsford C. Salmon: fast and bias-aware  
1307 quantification of transcript expression using dual-phase inference. *Nat Methods*  
1308 2017;14:417–9. <https://doi.org/10.1038/nmeth.4197>.

1309 [107] Lin P, Troup M, Ho JWK. CIDR: Ultrafast and accurate clustering through imputation for  
1310 single-cell RNA-seq data. *Genome Biol* 2017;18:59. <https://doi.org/10.1186/s13059-017-1188-0>.

1312 [108] Lun AT, Bach K, Marioni JC. Pooling across cells to normalize single-cell RNA  
1313 sequencing data with many zero counts. *Genome Biol* 2016;17:75.  
1314 <https://doi.org/10.1186/s13059-016-0947-7>.

1315 [109] Lovell DR, Chua X-Y, McGrath A. Counts: an outstanding challenge for log-ratio analysis  
1316 of compositional data in the molecular biosciences. *NAR Genomics Bioinforma*  
1317 2020;2:lqaa040. <https://doi.org/10.1093/nargab/lqaa040>.

1318 [110] Gene Ontology Resource. Gene Ontol Resour n.d. <http://geneontology.org/> (accessed  
1319 March 10, 2022).

1320 [111] Klopfenstein DV, Zhang L, Pedersen BS, Ramírez F, Warwick Vesztrocy A, Naldi A, et al.  
1321 GOATOOLS: A Python library for Gene Ontology analyses. *Sci Rep* 2018;8:1–17.  
1322 <https://doi.org/10.1038/s41598-018-28948-z>.

1323 [112] Benjamini Y, Hochberg Y. Controlling the False Discovery Rate: A Practical and Powerful  
1324 Approach to Multiple Testing. *J R Stat Soc Ser B Methodol* 1995;57:289–300.

1325 [113] Csardi G, Nepusz T. The Igraph Software Package for Complex Network Research.  
1326 *InterJournal* 2005;Complex Systems:1695.

1327 [114] Hagberg AA, Schult DA, Swart PJ. Exploring network structure, dynamics, and function  
1328 using NetworkX. In: Varoquaux G, Vaught T, Millman J, editors. *Proc. 7th Python Sci.*  
1329 Conf., Pasadena, CA USA: 2008, p. 11–5.

147

1330 [115] Korotkevich G, Sukhov V, Budin N, Shpak B, Artyomov MN, Sergushichev A. Fast gene  
1331 set enrichment analysis 2021:060012. <https://doi.org/10.1101/060012>.

1332 [116] Wu T, Hu E, Xu S, Chen M, Guo P, Dai Z, et al. clusterProfiler 4.0: A universal  
1333 enrichment tool for interpreting omics data. The Innovation 2021;2:100141.  
1334 <https://doi.org/10.1016/j.xinn.2021.100141>.

1335 [117] Love MI, Huber W, Anders S. Moderated estimation of fold change and dispersion for  
1336 RNA-seq data with DESeq2. Genome Biol 2014;15:550. <https://doi.org/10.1186/s13059-014-0550-8>.

1338 [118] Shen X-X, Opulente DA, Kominek J, Zhou X, Steenwyk JL, Buh KV, et al. Tempo and  
1339 Mode of Genome Evolution in the Budding Yeast Subphylum. Cell 2018;175:1533-1545.e20. <https://doi.org/10.1016/j.cell.2018.10.023>.

1341 [119] Camacho C, Coulouris G, Avagyan V, Ma N, Papadopoulos J, Bealer K, et al. BLAST+:  
1342 architecture and applications. BMC Bioinformatics 2009;10:421.  
1343 <https://doi.org/10.1186/1471-2105-10-421>.

1344 [120] Yu G, Li F, Qin Y, Bo X, Wu Y, Wang S. GOSemSim: an R package for measuring  
1345 semantic similarity among GO terms and gene products. Bioinformatics 2010;26:976–8.  
1346 <https://doi.org/10.1093/bioinformatics/btq064>.

1347 [121] R Core Team. R: A Language and Environment for Statistical Computing. Vienna,  
1348 Austria: R Foundation for Statistical Computing; 2017.

1349